Received: 7 July 2023 | Revised: 3 November 2023 | Accepted: 7 January 2024

DOI: 10.1002/cnm.3803

SPECIAL ISSUE ARTICLE

WILEY

Tube law parametrization using in vitro data for one-dimensional blood flow in arteries and veins

TUBE LAW PARAMETRIZATION IN ARTERIES AND VEINS

Chiara Colombo[1] | **Annunziato Siviglia**[1] | **Eleuterio F. Toro**[2] | **Daniel Bia**[3] | **Yanina Zócalo**[3] | **Lucas O. Müller**[4]

[1]Department of Civil, Environmental and Mechanical Engineering, University of Trento, Trento, Italy

[2]Laboratory of Applied Mathematics, DICAM, University of Trento, Trento, Italy

[3]Department of Physiology, Faculty of Medicine, University of the Republic, Montevideo, Uruguay

[4]Department of Mathematics, University of Trento, Trento, Italy

Correspondence

Chiara Colombo, Department of Civil, Environmental and Mechanical Engineering, University of Trento, Via Mesiano 77, Trento 38123, Italy.

Email: chiara.colombo-1@unitn.it

Funding information

the Italian Ministry of Education, Universities and Research (MUR), in the framework of the project DICAM-EXC (Departments of Excellence 2023-2027)

Abstract

The deformability of blood vessels in one-dimensional blood flow models is typically described through a pressure-area relation, known as the tube law. The most used tube laws take into account the elastic and viscous components of the tension of the vessel wall. Accurately parametrizing the tube laws is vital for replicating pressure and flow wave propagation phenomena. Here, we present a novel mathematical-property-preserving approach for the estimation of the parameters of the elastic and viscoelastic tube laws. Our goal was to estimate the parameters by using ovine and human in vitro data, while constraining them to meet prescribed mathematical properties. Results show that both elastic and viscoelastic tube laws accurately describe experimental pressure-area data concerning both quantitative and qualitative aspects. Additionally, the viscoelastic tube law can provide a qualitative explanation for the observed hysteresis cycles. The two models were evaluated using two approaches: (i) allowing all parameters to freely vary within their respective ranges and (ii) fixing some of the parameters. The former approach was found to be the most suitable for reproducing pressure-area curves.

KEYWORDS

1D model, blood flow equations, collapsible tubes, in vitro data, tube law parametrization

1 | INTRODUCTION

In silico models have become increasingly important in modern medical research as a means of simulating and quantifying pressure and flow pulse waveforms in the circulatory system,[1] since they can simulate the behavior of the circulatory system under both healthy and pathological conditions.[2,3] Among all the mathematical models used to describe the cardiovascular system, an important role is played by one-dimensional (1D) models, which have shown to provide accurate prediction of pressure and flow wave propagation on large arterial and venous networks.[3–7] These models are governed by systems of evolutionary partial differential equations (PDEs) of hyperbolic or hyperbolic-dominant type, and provide a reasonable balance between computational cost and accuracy.[8]

These models consider the deformability of blood vessels by incorporating the so-called *tube law*, which relates the blood pressure to the wall tension. In turn, wall tension is normally described in terms of strain, for purely elastic models, and in terms of strain and strain rate for viscoelastic models.[9] This coupling of fluid dynamics with vessel's mechanical properties depends on the composition of the vessel wall, which in turn is determined by its function.[10] While tube laws used in 1D models can consider several different phenomena contributing to the wall tension,[11] in this work we focus on elastic and viscoelastic tube laws, which in turn are the most common used ones. Elastic tube laws (elastic models) consider a purely elastic response to the vessel wall to deformation,[6,12,13] while viscoelastic tube laws (viscoelastic models) consider a viscoelastic response, incorporating the viscous properties of the vessel wall neglected in elastic models.[9,11,14,15]

Both elastic and viscoelastic tube laws are characterized by parameters that represent vessels' geometrical and mechanical properties.[9,16] These parameters are typically derived from more complex models,[17] or by analyzing temporal data for pressure-area dynamics, which are obtained from in vitro or in vivo experiments. By utilizing this data, it is possible to extract the values of the parameters associated with a specific formulation (either elastic or viscoelastic) and use them to evaluate the model's ability to reproduce real wave patterns[4,7] and study structural and functional differences among vessels.[18-20] However, parameter values cannot be arbitrary. Certain constrains are derived from physical considerations, while others might be needed if specific mathematical properties of the 1D blood flow model are required. Elastic models are typically governed by quasi-linear first-order PDE systems, where the parameters of the tube law are chosen such that the model is of hyperbolic type,[15,21,22] allowing for the use of numerical methods of the Godunov type.[23] Other approaches are also available. Elastic models can indeed be linearized and a solution, either analytical or semi-analytical, can be found in terms of Fourier series expansions.[24,25] Viscoelastic models are usually governed by quasi-linear second-orders PDEs systems of parabolic type[4,11] and can be solved applying different numerical approaches. One approach consists in using the Galerkin method, where the solution is expanded in terms of a set of basis functions, and the equations are projected onto these functions to obtain a system of algebraic equations.[4,26] Another approach consists in using the operator splitting technique, where the original problem is split into a convective and a diffusive subproblem that are solved sequentially.[11,23] A third alternative approach is to transform the initial parabolic problem into an hyperbolic problem using the Cattaneo's relaxation approach.[27] This third method has been effectively applied to viscoelastic models,[28,29] and enables the use of standard Godunov-type numerical methods.

In this work we assess how constraining tube law parameters to obtain certain mathematical properties of 1D blood flow model affects the capacity of the tube law to fit experimental data. Specifically, we consider two widely employed tube laws, the elastic tube law as described in Pedley et al.[13] and the viscoelastic tube law as described in Alastruey et al.[4] For the estimation procedure we use in vitro pressure and area time series extracted from ovine and human donors. These estimates must not only satisfy physiological requirements to correctly reproduce pressure waveforms, but also ensure that the mathematical nature (namely hyperbolicity and genuine non-linearity characteristic fields)[23] of the 1D blood flow model is preserved. To this end, since elastic and viscoelastic tube laws give rise to hyperbolic and parabolic systems of PDEs, respectively, we reformulate the parabolic problem as an hyperbolic system following Montecinos et al.[28] We then study the mathematical properties of the two systems of PDEs and ensure that the structure of the PDE systems is strictly hyperbolic with genuinely non-linear and/or linearly degenerate characteristic fields. These properties ensure the well posedness of certain initial- and initial-boundary value problems involving these 1D blood flow models.[30]

2 | MATERIALS AND METHODS

2.1 | Mathematical model for blood flow in collapsible tubes

We consider the impermeable and deformable tubular control volume showed in Figure 1 and assume a Newtonian incompressible fluid flowing in the axial direction x with an axisymmetric velocity profile. In such conditions, 1D blood flow in major vessels is described by two PDEs, representing mass conservation and momentum balance. The model reads

$$\begin{cases} \partial_t A + \partial_x q = 0, \\ \partial_t q + \partial_x \left(\dfrac{q^2}{A} \right) + \dfrac{A}{\rho} \partial_x p = f, \end{cases} \tag{1}$$

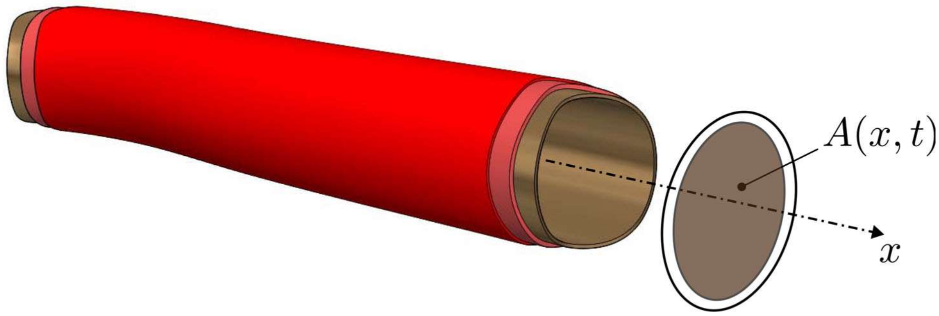

FIGURE 1 **Vessel configuration.** Axially symmetric vessel configuration in three space dimensions at time t, with an indication of the cross-sectional area $A(x,t)$. The vessel wall consists of three layers: the tunica intima (in brown), the tunica media (light red) and the tunica adventitia (in red). Each of these layers has a specific role. The function of the tunica media is to supply mechanical strength and contractile power to the vessel. Therefore, it is predominantly composed of smooth muscle cells, immersed in a matrix of elastin and collagen fibers. More details about the tunica media can be found in Levick[31] and in Burton,[10] together with more information on the roles of the other layers and their composition.

where x is the axial coordinate along the vessel (Figure 1) and t is the time. The unknowns are the cross-sectional area of the vessel lumen $A(x,t) \in \mathbb{R}^+ \setminus \{0\}$, the flow rate $q(x,t) \in \mathbb{R}$ and the cross-sectional averaged internal pressure $p(x,t) \in \mathbb{R}$. The friction term f, depends on the local velocity profile which is assumed a priori, while ρ is the blood density.

System (1) has more unknowns than equations, hence a closure condition must be introduced. This closure condition is given by the tube law, which relates the averaged internal pressure $p(x,t)$ to the cross-sectional area $A(x,t)$.

2.2 | The elastic model

Here we adopt an elastic tube law[12,13,22,32] of the form

$$p(x,t) = p_{ext}(x,t) + \psi(A(x,t);A_0,K,m,n,p_0), \tag{2}$$

where $p_{ext}(x,t)$ is the external pressure, assumed equal to zero. $\psi(A(x,t);A_0,K,m,n,p_0)$ represents the elastic component of the tube law and is given by

$$\psi(A(x,t);A_0,K,m,n,p_0) = K\phi(A(x,t);A_0,m,n) + p_0, \tag{3}$$

with

$$\phi(A(x,t);A_0,m,n) = \left[\left(\frac{A(x,t)}{A_0}\right)^m - \left(\frac{A(x,t)}{A_0}\right)^n\right]. \tag{4}$$

In this work, all the parameters are considered constant in space and time. Particularly, $A_0 \in \mathbb{R}^+ \setminus \{0\}$ denotes the cross-sectional area at equilibrium, $K \in \mathbb{R}^+ \setminus \{0\}$ represents the stiffness coefficient of the vessel wall, $p_0 \in \mathbb{R}$ is the reference cross-sectional averaged pressure, while parameters $m \in \mathbb{R}$ and $n \in \mathbb{R}$ intend to mimic the hyperelastic nature of vessel walls and the behavior during collapse, respectively.

The adopted tube law allows to describe experimentally observed pressure-area relations over a wide pressure range. These relations are determined by the biological composition of the wall of vessels,[10] which contains elastine, collagen fibers and smooth muscle cells. It is well known that, for increasing positive transmural pressures $(p_{tm}(x,t) = p(x,t) - p_0)$, the stiffness of vessels raise, due to the gradual recruitment of collagen fibers, determining a characteristic hyperelastic behavior. On the other hand, for negative transmural pressures, vessels will undergo collapse, resulting in the buckling of the vessel wall and the consequent increment in stiffening for decreasing transmural pressures. The intermediate region between the collapse-related buckling region and the hyperelastic one, is a range where the vessel exhibits maximum compliance (or minimal stiffness). Further details on this subject are available in Caro[33] and Fung.[34]

2.2.1 | Governing equations

We consider a mathematical model consisting of system (1), along with tube law (2). Since we are interested in the eigenstructure of the resulting system, we will restrict our study to the homogeneous case. The resulting system can be written in quasi-linear form as follows

$$\partial_t \boldsymbol{Q} + \boldsymbol{B}(\boldsymbol{Q})\partial_x \boldsymbol{Q} = \boldsymbol{0}, \tag{5}$$

where the vector of unknowns $\mathbf{Q}$ is

$$\mathbf{Q} = [A, q]^T \in \Omega, \tag{6}$$

with

$$\Omega = \{(A,q) \in \mathbb{R}^+ \setminus \{0\} \times \mathbb{R}\}. \tag{7}$$

The matrix of coefficients $\mathbf{B}(\mathbf{Q})$ is given by

$$\mathbf{B}(\mathbf{Q}) = \begin{bmatrix} 0 & 1 \\ c_E^2 - u^2 & 2u \end{bmatrix}, \tag{8}$$

where $u = q/A$, and

$$c_E = \sqrt{\frac{A}{\rho} K \partial_A \phi} \tag{9}$$

is the wave speed. Next we study some mathematical properties of system (5).

2.2.2 | Eigenstructure

The eigenstructure of system (5) is given by the eigenvalues and the corresponding eigenvectors of coefficient matrix (8). Eigenvalues of matrix (8) are

$$\lambda_1 = u - c_E \quad \text{and} \quad \lambda_2 = u + c_E. \tag{10}$$

The corresponding right eigenvectors are

$$\mathbf{R}_1(\mathbf{Q}) = \begin{bmatrix} 1 \\ u - c_E \end{bmatrix}, \quad \text{and} \quad \mathbf{R}_2(\mathbf{Q}) = \begin{bmatrix} 1 \\ u + c_E \end{bmatrix}. \tag{11}$$

The mathematical nature of this model depends on parameters m and n of the elastic tube law (2).[21,22] System (5) is strictly hyperbolic if λ_1 and λ_2 are real and distinct. Since $u \in \mathbb{R}$, we need to check if $c_E \in \mathbb{R}^+ \setminus \{0\}$. Therefore, we need to verify that the argument of the squared root of the wave speed (9) is positive. Since $A>0$, $\rho>0$, $K>0$ for physical reasons, we only need to verify that

$$\partial_A \phi > 0. \tag{12}$$

Simple manipulations give

$$m\left(\frac{A}{A_0}\right)^m > n\left(\frac{A}{A_0}\right)^n. \tag{13}$$

Introducing $a = A/A_0$, we write inequality (13) as

$$m(a)^m > n(a)^n. \tag{14}$$

We see that

- if $a<1$, then

  I) if $m,n>0$, then for a given m, $\exists \nu_1,\nu_2 \in \mathbb{R}^+ \setminus \{0\}$ s.t. $n \in (0,\nu_1) \cup (\nu_2,+\infty)$,
  II) if $m \le 0, n \ge 0$, then there is no solution,
  III) if $m,n<0$, then inequality (14) holds true only if $n<m$,
  IV) if $m>0, n\le 0$, then inequality (14) holds always true,

- if $a>1$, then

  I) if $m,n>0$, then inequality (14) holds true only if $n<m$,
  II) if $m \le 0, n \ge 0$, then there is no solution,
  III) if $m,n<0$, then for a given m, $\exists \nu_3,\nu_4 \in \mathbb{R}^- \setminus \{0\}$ s.t. $n \in [\nu_3,\nu_4]$,
  IV) if $m>0, n\le 0$, then inequality (14) holds always true,

- if $a=1$, then

  I) if $m,n>0$, then inequality (14) holds true only if $n<m$,
  II) if $m \le 0, n \ge 0$, then there is no solution,
  III) if $m,n<0$, then inequality (14) holds true only if $n<m$,
  IV) if $m>0, n\le 0$, then inequality (14) holds always true.

Figure 2 displays a graphical example of the previous cases, while the full derivation of the above conclusions can be seen in Colombo.[35] Figure 2 shows contour plots with binary output of the function $y(m,n;a) = m(a)^m - n(a)^n$, where the black regions represent the sectors where inequality (14) holds true for the given $a>0$ and the given combination of m and n. Since inequality (14) must hold true $\forall a>0$, all the previous cases must be satisfied simultaneously. Combining them (Figure 2F), we obtain that our system is strictly hyperbolic when

$$m>0 \quad \text{and} \quad n \le 0. \tag{15}$$

2.2.3 | Characteristic fields

Parameters m and n control which are the families of waves present in the solution of system (5). In particular, genuinely non-linear characteristic fields will give rise to shocks or rarefactions, while linearly degenerate characteristic fields generate contact discontinuities.[23] Genuine non-linearity is a desirable property of hyperbolic systems of conservation laws. In fact, problems involving genuinely non-linear characteristic fields are significantly easier to analyze and

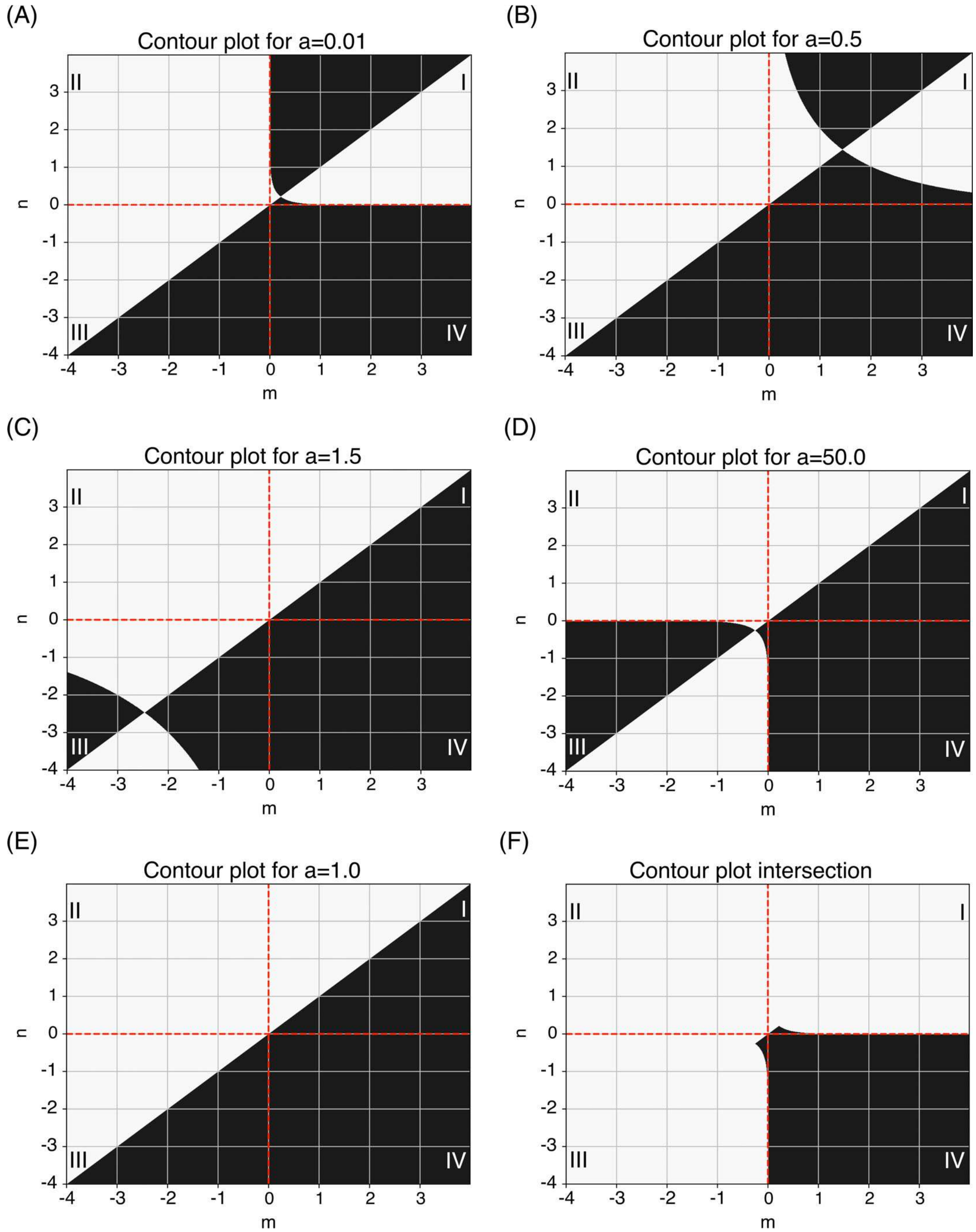

FIGURE 2 **Contour plots with binary output.** Panels (A)–(E) display different contour plots with binary output of the function $y(m,n;a) = m(a)^m - n(a)^n$ for 5 given $a > 0$. Panel (F) displays a contour plot with binary output obtained by intersecting the previous 5 panels. Black sections are regions where $y(m,n;a) > 0$. It is worth remarking that the mismatch between the analytical solution and the results in panel (F) (small spots in quadrants I and III) is due to the particular choice we made for a. A perfect match could be obtained by selecting $a \to 0$ and $a \to \infty$.

discretize with respect to problems that present non genuinely non-linear characteristic fields. As a consequence, most general well-posedness results for initial value problems regarding hyperbolic systems of partial differential equations are available for systems having either genuinely non-linear or linearly degenerate characteristic fields.[30] Characteristic fields are said to be genuinely non-linear if the following inequalities are fulfilled

$$\nabla\lambda_1(\mathbf{Q}) \cdot \mathbf{R}_1(\mathbf{Q}) < 0 \quad \forall \mathbf{Q} \in \Omega, \tag{16a}$$

$$\nabla\lambda_2(\mathbf{Q})\cdot\mathbf{R}_2(\mathbf{Q})>0 \quad \forall\mathbf{Q}\in\Omega, \tag{16b}$$

where $\nabla\lambda_i(\mathbf{Q})$ is the gradient of λ_i. Particularly, for the problem under consideration the following holds

$$\nabla\lambda_i(\mathbf{Q})\cdot\mathbf{R}_i(\mathbf{Q})=\left(\frac{\partial}{\partial A}\lambda_i+\lambda_i\frac{\partial}{\partial q}\lambda_i\right),\quad i=1,2. \tag{17}$$

Expressing the partial derivatives, relation (17) becomes

$$\begin{aligned}\nabla\lambda_i(\mathbf{Q})\cdot\mathbf{R}_i(\mathbf{Q})&=\pm\frac{K}{2\rho c_E}\left(3\partial_A\phi+A\partial_A^{(2)}\phi\right)=\\&=\pm\frac{K}{2\rho c_E A}\left[m(m+2)\left(\frac{A}{A_0}\right)^m-n(n+2)\left(\frac{A}{A_0}\right)^n\right],\quad i=1,2.\end{aligned} \tag{18}$$

Under the assumption that $m>0$, $n\le 0$, since $K>0$, $\rho>0$, $c_E>0$, $A>0$, $A_0>0$, we need to solve the following inequality

$$m(m+2)\left(\frac{A}{A_0}\right)^m-n(n+2)\left(\frac{A}{A_0}\right)^n>0. \tag{19}$$

Introducing again $a=A/A_0$, we write inequality (19) as

$$m(m+2)(a)^m-n(n+2)(a)^n>0. \tag{20}$$

It is possible to show that

- if $a<1$, then for a given m, $\exists\nu_5\in[-m-2,-2)$ s.t. $n\in[\nu_5,0]$,
- if $a>1$, then for a given m, $\exists\nu_6<-2$ s.t. $n\in(\nu_6,0]$,
- if $a=1$, then for a given m, $n\in[-m-2,0]$.

These three cases must be satisfied simultaneously, thus their combination gives

$$m>0 \quad\text{and}\quad n\in[-2,0]. \tag{21}$$

Conditions (21) for parameters m and n guarantee that the 1D elastic model is strictly hyperbolic and its characteristic fields are genuinely non-linear.

2.3 | The viscoelastic model

Here we adopt the following viscoelastic tube law[4,11,15,36]

$$p(x,t)=p_{ext}(x,t)+\psi(A(x,t);A_0,K,m,n,p_0)+\varphi(A(x,t);A_0,\Gamma)\partial_t A, \tag{22}$$

where the term involving $\partial_t A$ with

$$\varphi(A(x,t);A_0,\Gamma)=\frac{\Gamma}{A_0\sqrt{A(x,t)}}, \tag{23}$$

represents its viscous component. $\Gamma\in\mathbb{R}^+$ is a parameter related to the viscosity of the vessel wall,[4] assumed constant in space and time.

2.3.1 | Governing equations

We consider the 1D blood flow model consisting of system (1), along with tube law (22). The resulting system can be reformulated following the procedure exposed in Montecinos et al[28,29] to obtain an hyperbolic system of PDEs. Specifically, we introduce a new variable $\Psi \in \mathbb{R}$ and a relaxation parameter $\varepsilon \in \mathbb{R}^+ \setminus \{0\}$ as well as the following additional evolutionary equation for Ψ

$$\partial_t \Psi = \frac{1}{\varepsilon}(\partial_x q - \Psi). \tag{24}$$

This results in the following property

$$\Psi \rightarrow \partial_x q, \quad \text{as} \varepsilon \rightarrow 0, \tag{25}$$

so that one can recover the original parabolic problem for small relaxation parameter ε. We then formulate the viscoelastic tube law (22) as

$$p(x,t) = p_{ext}(x,t) + \psi(A(x,t);A_0,K,m,n,p_0) - \varphi(A(x,t);A_0,\Gamma)\Psi. \tag{26}$$

Finally we write the system in quasi-linear form as in (5). The vector of unknowns is

$$\mathbf{Q} = [A,q,\Psi]^T, \tag{27}$$

and the matrix of coefficients is

$$\mathbf{B}(\mathbf{Q}) = \begin{bmatrix} 0 & 1 & 0 \\ c_V^2 - u^2 & 2u & -\dfrac{A}{\rho}\varphi \\ 0 & -\dfrac{1}{\varepsilon} & 0 \end{bmatrix}, \tag{28}$$

where

$$c_V = \sqrt{c_E^2 + \frac{\varphi\Psi}{2\rho}} = \sqrt{\frac{A}{\rho}K\partial_A\phi + \frac{\varphi\Psi}{2\rho}} \tag{29}$$

is the wave speed. System (5) with (24) and (25) constitutes a relaxation system whose solutions approximate those of the original viscoelastic system.

2.3.2 | Eigenstructure

The eigenstructure of the system is given by the eigenvalues of matrix (28) and the corresponding eigenvectors. The eigenvalues are

$$\lambda_1 = u - \widetilde{c}, \quad \lambda_2 = 0, \quad \lambda_3 = u + \widetilde{c}, \tag{30}$$

where the wave speed is

$$\widetilde{c} = \sqrt{c_V^2 + \frac{A\varphi}{\rho\varepsilon}} = \sqrt{\frac{A}{\rho}K\partial_A\phi + \frac{\varphi\Psi}{2\rho} + \frac{A\varphi}{\rho\varepsilon}}. \tag{31}$$

The right eigenvectors are

$$\mathbf{R}_1(\mathbf{Q}) = \begin{bmatrix} 1 \\ u-\widetilde{c} \\ -1/\varepsilon \end{bmatrix}, \quad \mathbf{R}_2(\mathbf{Q}) = \begin{bmatrix} 1 \\ 0 \\ \dfrac{(c_V^2-u^2)\rho}{\varphi A} \end{bmatrix}, \quad \mathbf{R}_3(\mathbf{Q}) = \begin{bmatrix} 1 \\ u+\widetilde{c} \\ -1/\varepsilon \end{bmatrix}. \tag{32}$$

The eigenstructure allows us to study the hyperbolicity of the system, as we did for the elastic model. Specifically, it is possible to prove that the system of conservation laws is strictly hyperbolic, that is, the eigenvalues are real and distinct, if

$$\frac{A}{\rho}K\partial_A\phi + \frac{\varphi\Psi}{2\rho} + \frac{A\varphi}{\rho\varepsilon} > 0. \tag{33}$$

After some algebraic manipulations, we obtain that inequality (33) is equivalent to

$$\frac{\partial p}{\partial A} - \frac{1}{\varepsilon}\frac{\partial p}{\partial \Psi} > 0. \tag{34}$$

However we cannot identify any mathematical constrains on the parameters since relation (34) has not a closed form. We observe that if $\varphi > 0$, then

$$\frac{\partial p}{\partial \Psi} = -\varphi < 0. \tag{35}$$

Thus, we can always choose a $\varepsilon > 0$ small enough such that inequality (34) is satisfied and the system is strictly hyperbolic, independently of the sign of $\frac{\partial p}{\partial A}$. Additionally, since the viscoelastic tube law (22) is an extension of the elastic tube law (2), we also observe that we are able to resume the properties of the elastic model when the viscoelasticity coefficient is set to zero. Specifically, we have that the elastic component of the viscoelastic tube law is a monotonically increasing function of the cross-sectional area A, that is,

$$\left.\left(\frac{\partial p}{\partial A} - \frac{1}{\varepsilon}\frac{\partial p}{\partial \Psi}\right)\right|_{\varphi=0} = \left.\frac{\partial p}{\partial A}\right|_{\varphi=0} = \frac{\partial \psi}{\partial A} = K\partial_A\phi > 0, \tag{36}$$

which is equivalent to condition (12).

2.3.3 | Characteristic fields

Here we analyze the nature of the characteristic fields. It is easy to see that λ_2-characteristic field is linearly degenerate. Instead, it is possible to prove that λ_1-, λ_3-characteristic fields are genuinely non-linear. It holds

$$\nabla\lambda_i(\mathbf{Q})\cdot\mathbf{R}_i(\mathbf{Q}) = \left(\frac{\partial}{\partial A}\lambda_i + \lambda_i\frac{\partial}{\partial q}\lambda_i - \frac{1}{\varepsilon}\frac{\partial}{\partial \Psi}\lambda_i\right), \quad i = 1,3. \tag{37}$$

Computing the partial derivatives, relation (37) becomes

$$\nabla\lambda_i(\mathbf{Q})\cdot\mathbf{R}_i(\mathbf{Q})=\pm\left(\frac{\partial\widetilde{c}}{\partial A}+\frac{\widetilde{c}}{A}-\frac{1}{\varepsilon}\frac{\partial\widetilde{c}}{\partial\Psi}\right),\quad i=1,3. \tag{38}$$

If we rewrite the expression of $\widetilde{c}$ (31) as follows

$$\widetilde{c}=\sqrt{\frac{A}{\rho}K\partial_A\phi+\frac{\varphi\Psi}{2\rho}+\frac{A\varphi}{\rho\varepsilon}}=\sqrt{\frac{A}{\rho}\frac{\partial p}{\partial A}-\frac{A}{\rho\varepsilon}\frac{\partial p}{\partial\Psi}}=\sqrt{c_V^2-\frac{A}{\rho\varepsilon}\frac{\partial p}{\partial\Psi}}, \tag{39}$$

expression (38) becomes

$$\boldsymbol{\nabla}\lambda_i(\mathbf{Q})\cdot\mathbf{R}_i(\mathbf{Q})=\pm\left(\frac{c_V}{\widetilde{c}}\frac{\partial c_V}{\partial A}-\frac{1}{2\widetilde{c}}\frac{1}{\rho\varepsilon}\frac{\partial p}{\partial\Psi}-\frac{1}{2\widetilde{c}}\frac{A}{\rho\varepsilon}\frac{\partial^2 p}{\partial\Psi\partial A}+\frac{\widetilde{c}}{A}-\frac{1}{\varepsilon}\frac{c_V}{\widetilde{c}}\frac{\partial c_V}{\partial\Psi}\right),\quad i=1,3. \tag{40}$$

Noting that

$$\frac{\partial c_V}{\partial\Psi}=\frac{1}{2c_V}\frac{A}{\rho}\frac{\partial^2 p}{\partial\Psi\partial A}, \tag{41}$$

and that

$$\frac{\partial p}{\partial\Psi}=-\varphi,\quad \frac{\partial^2 p}{\partial\Psi\partial A}=\frac{\varphi}{2A}, \tag{42}$$

we obtain

$$\boldsymbol{\nabla}\lambda_i(\mathbf{Q})\cdot\mathbf{R}_i(\mathbf{Q})=\pm\left(\frac{c_V}{\widetilde{c}}\frac{\partial c_V}{\partial A}+\frac{\widetilde{c}}{A}\right). \tag{43}$$

Since $\widetilde{c}>0$, we need to prove that

$$c_V\frac{\partial c_V}{\partial A}+\frac{\widetilde{c}^2}{A}>0. \tag{44}$$

Recalling the expression of the wave speed $\widetilde{c}$ (31), where it appears as denominator the relaxation parameter ε, we conclude that, under the assumption that the system is strictly hyperbolic, we can always choose $\varepsilon>0$ small enough such that inequality (44) is fulfilled and λ_1-, λ_3-characteristic fields are genuinely non-linear. Hence, the parameters have no explicit mathematical constraints, only needing to satisfy physiological ones. As a result, we can reduce the hypotheses on the fitting parameters, with respect to the elastic model, because the viscoelastic model preserves its nature even when we relax conditions (12) (or equivalently (15)) and consider $m\in\mathbb{R}$ and $n\in\mathbb{R}$.

2.4 | Tube law parameter estimation

We are interested in estimating parameters K,m,n,Γ of tube laws (2) and (22) by fitting ovine and human in vitro data. Here, we introduce the in vitro data and we describe the methodology that we used for the evaluation of the parameters.

2.4.1 | In vitro data

The experimental data used in this study[9,18,37] consist of multiple sets of pressure-diameter time series acquired from 12 adult sheep and from 15 humans.

All protocols applied to record the data were approved by the Research and Development Council of the Universidad de la Republica (Uruguay) and were conducted in accordance with the guide for the care and use of laboratory animals.[38]

For all the data (ovine and human), pressure values (in mmHg) have been recorded through the usage of a solid-state microtransducer (Model P2.5, 1200 Hz frequency response; Konigsberg Instruments, Pasadena, CA, USA). Vascular diameters have been measured with a pair of ultrasonic gauges (5 MHz; 2 mm diameter) sutured to the adventitia. A sonomicrometer (Triton Technology Inc., San Diego, CA, USA) has been used to convert transit time (1580 m/s) to distance.

The measures of ovine data have been taken in different vessels: seven arteries of the systemic circulation, that is, carotid artery (CA), brachiocephalic trunk (BT), ascending aorta (AA), proximal descending aorta (PDA), medial descending aorta (MDA), distal descending aorta (DDA) and femoral artery (FA), two arteries of the pulmonary circulation, that is, main pulmonary artery (PT) and left pulmonary artery (LPA), and four veins, that is, inferior vena cava (VCI), superior vena cava (VCS), jugular vein (VJ) and femoral vein (VF) (Figure 3). In vitro tests for ovine arteries have been carried out at physiological pressure, while ovine veins have been tested under both low (L—physiological) and high (H—arterial values range) pressure.[9,37] The aforementioned prefixes shall be utilized henceforth in the text, tables, and illustrations to specify the data that is being referenced. The methodology used to record ovine data can be divided into two parts.[9,37,39] Firstly, the animals have been anesthetized and segments of the selected vessels have been delimited in vivo using two suture stitches. Following this, pressure and diameter sensors have been instrumented on each segment before excision, and in vivo data have been subsequently collected. During the second phase, the sheep have been euthanized and their instrumented segments have been carefully removed and mounted in custom cannulae within the flow circuit (in vitro system). They have been then immersed and perfused with oxygenated Tyrode's solution at a temperature of 37°C and a pH of 7.4. The same in vivo vessels' length has been maintained in the process. After a period of adaptation of 15 min, in vitro measures of pressure and diameter have been gathered. Pressure and diameter signals from 10 to 20 consecutive cycles have been sampled simultaneously every 5 ms (sampling rate = 200 Hz). Pressure levels and stretch rates ("heart rate") similar to those observed in sheep have been chosen. The previously acquired in vivo data have been used to confirm the adequate quality of the diameter and pressure signals and to generate in vitro pressure waveforms that simulate the morphology of the pressure waveforms found in vivo.

For both human and sheep data, pressure values (in mmHg) and diameter values (in mm) were recorded under dynamic conditions. The recordings for human data have been done for two types of vessels at high pressure: saphenous vein (Saf) and femoral artery (Fem). These segments have been obtained from donors in a condition of brain death with aseptic surgical techniques, during multiple organ and tissue harvesting.[18] The methodology utilized to record this data is comparable to that used for ovine data.[39] Prior to vessels removal, the segments have been measured and marked with two suture stitches. Subsequently, they have been cut off and fitted onto the same in vitro setup for biomechanical testing. Throughout this process, efforts have been made to maintain the length of the in vivo vessels.

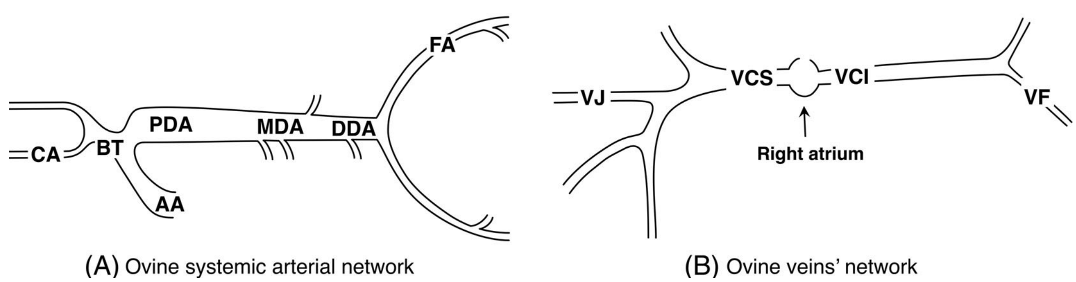

FIGURE 3 Schematic representation of the ovine vessels' network, with the indication of the main vessels. Panel (A) on the left, the ovine systemic arterial network. AA, ascending aorta; BT, brachiocephalic trunk; CA, carotid artery; DDA, distal descending aorta; FA, femoral artery; MDA, medial descending aorta; PDA, proximal descending aorta. Panel (B) on the right, the ovine veins' network. VCI, inferior vena cava; VCS, superior vena cava; VF, femoral vein; VJ, jugular vein. Adapted from Battista et al.[16] and Zócalo et al.[37]

Pressure and diameter signals from 10 to 20 consecutive cycles have been simultaneously sampled every 5 ms (sampling rate = 200 Hz), using pressure levels and stretch rates ("heart rate") similar to those observed in humans.

A typical example of the acquired in vitro data is shown in Figure 4A.

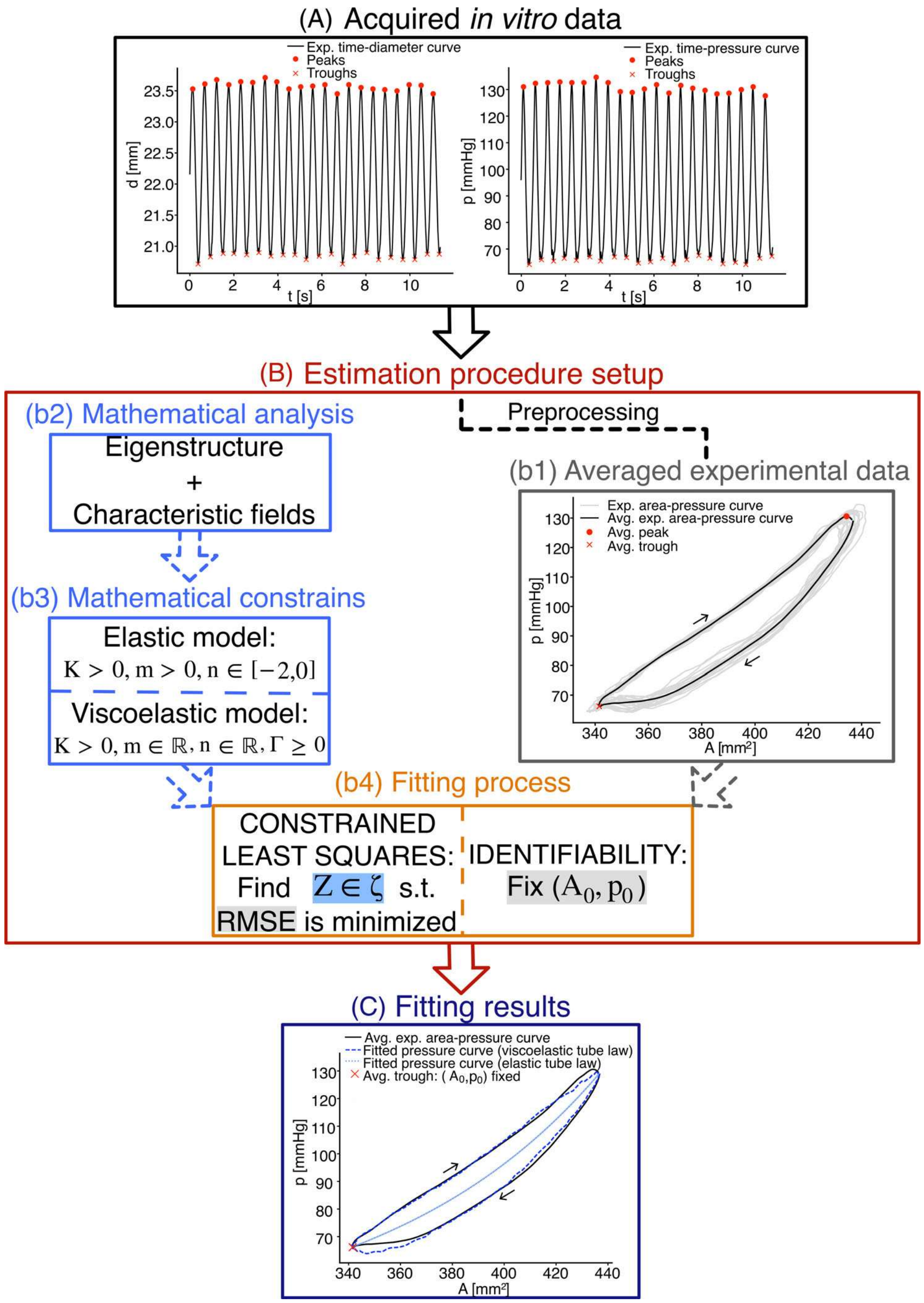

FIGURE 4 **Conceptual scheme of the methodology used for the parameter estimation process.** Overview of the process showing the input, which is an example of acquired in vitro data (A), the estimation procedure (B) to pass from the input to the output, and the output, which is the final fitting result (C). The estimation procedure (B) is composed of different steps. A phase of preprocessing of the acquired in-vitro data is used to obtain the averaged experimental data (b1). Instead the mathematical analysis (b2) of the two considered models is used to ensure that the mathematical properties of the models in which we are interested are preserved, through mathematical constrains (b3) on the parameters that must be fulfilled. All these steps are then used in the fitting process (B4) that gives us the final results. Specifically, it focuses on two aspects. Firstly, we fix A_0 and p_0 to enhance the identifiability of the other parameters. Secondly, the other parameters, which are represented by the vector $\mathbf{Z} = [K, m, n, \Gamma]$, were determined through minimizing the root mean squared errors (RMSE). The range ζ within which the parameters must fall is outlined in Table 2.

TABLE 1 Statistics of A_0 and p_0.

		A0 [mm^2]			*p0* [mmHg]		
Vess.	**Num.**[a]	**Min.**	**Avg.**	**Max.**	**Min.**	**Avg.**	**Max.**
Sheep systemic arteries							
AA	12	289.58	365.01	415.86	63.01	68.65	77.88
BT	11	248.83	304.80	489.15	60.79	66.78	74.08
CA	11	39.11	53.13	65.14	61.47	66.28	71.67
DDA	11	221.77	230.98	247.27	55.99	63.33	68.53
FA	11	21.87	26.60	32.64	61.63	67.97	72.84
MDA	11	247.50	267.49	279.74	54.88	63.52	69.43
PDA	11	263.78	284.87	294.97	59.28	65.31	71.68
Sheep pulmonary arteries							
LPA	11	138.93	179.45	242.89	9.91	12.14	14.85
PT	10	327.43	399.00	459.56	9.92	12.18	15.07
Sheep veins at high (H) pressure							
HVCI	5	255.39	318.32	377.11	63.32	70.12	74.31
HVCS	8	203.59	239.32	258.09	63.86	75.81	90.23
HVF	5	25.81	28.32	31.73	78.80	83.42	87.23
HVJ	8	67.99	152.54	258.11	67.14	79.96	101.16
Sheep veins at low (L) pressure							
LVCI	10	174.35	271.30	372.28	−2.13	1.73	4.07
LVCS	12	76.09	128.65	227.40	−0.68	2.39	6.97
LVF	30	19.62	27.32	42.22	0.55	10.39	28.64
LVJ	10	28.54	75.18	148.47	0.12	3.57	12.07
Human vessels							
Fem	30	23.69	43.90	55.53	54.93	73.58	107.24
Saf	20	27.11	41.37	48.46	52.81	68.61	102.03

Note: Minimum, average and maximum values in the averaged trough of the parameters A_0 and p_0 for all the vessel types (Vess.).
[a]Number of available sets of data for each type of vessel.

2.4.2 | Estimation procedure setup

Here, we detail the procedure utilized in our study to derive parameter estimates from in vitro data. Figure 4 shows a conceptual scheme of this process.

Starting from the acquired in vitro data (Figure 4A), we preprocessed all the pressure-diameter time series. Specifically, for each type of vessel we had several datasets containing the samples acquired (Table 1). Each of these datasets consisted of a time series of pressure and diameter values for more than a single cycle. For all the time series we have identified the peaks (red dots in Figure 4A) and the troughs (red crosses in Figure 4A) in the curves. The peaks are the moments of maximum pressure (diameter), while the troughs are the moments of minimum pressure (diameter). By identifying the peaks and troughs in the pressure-diameter time series, we extracted the data associated with individual cycles. We then calculated the mathematical mean over multiple cycles to obtain average signals. These averages are represented by an area-pressure loop, obtained considering the extracted pressures and the circular areas, whose diameters correspond to the extracted ones. These loops describe on average the behavior of the vessels along a single cardiac cycle. An example of such loops can be seen in Figure 4B1, where the gray curve represents the raw in vitro data, the black curve is the average signal, the red cross is the averaged trough, and the red dot is the averaged peak. The descending branch, connecting the averaged peak to the averaged trough, represents the relaxation phase. Here we observe a steep decrease of both pressure and vessel area. The ascending branch, connecting the averaged trough to the

TABLE 2 Parameter estimations summary.

Elastic tube law				
Case	K	m	n	Γ
E1	$K>0$	$m>0$	$n\in[-2,0]$	$\Gamma=0$
E2	$K>0$	$m=10.0$	$n=-1.5$	$\Gamma=0$
E3	$K>0$	$m=0.5$	$n=0.0$	$\Gamma=0$
E4	$K>0$	$m\in\mathbb{R}$	$n\in\mathbb{R}$	$\Gamma=0$
Viscoelastic tube law				
Case	K	m	n	Γ
V1	$K>0$	$m>0$	$n\in[-2,0]$	$\Gamma>0$
V2	$K>0$	$m=10.0$	$n=-1.5$	$\Gamma>0$
V3	$K>0$	$m=0.5$	$n=0.0$	$\Gamma>0$
V4	$K>0$	$m\in\mathbb{R}$	$n\in\mathbb{R}$	$\Gamma>0$

Note: The performed estimations have been summarized, with each case being identified by a specific name. The elastic tube law is represented by the letter E, while the viscoelastic tube law is represented by the letter V.

averaged peak, represents the loading phase. During this phase, pressure and area initially increase slowly due to vessel's compliance, then the increase becomes steep, as the vessels stiffen when subjected to higher pressures. The obtained averaged experimental data (Figure 4B1) were then saved and the fitting process (Figure 4B4) was applied to these averaged curves.

We now introduce the constrains derived from the mathematical analysis. Recalling that our goal is to fit experimental data while ensuring that the use of such parameters in 1D blood flow models results in hyperbolic mathematical problems with genuine nonlinear characteristic fields (Figure 4B3). As outlined in Sections 2.2.2 and 2.2.3, the parameters of the elastic tube law (2) have to satisfy the following mathematical constrains

$$K>0,\quad m>0 \quad \text{and} \quad n\in[-2,0]. \tag{45}$$

Similarly, in Sections 2.3.2 and 2.3.3, we demonstrated that the parameters of the viscoelastic tube law (22) have to fulfill the following constrains

$$K>0,\quad m\in\mathbb{R},\quad n\in\mathbb{R} \quad \text{and} \quad \Gamma\geq 0. \tag{46}$$

The fitting process is the final step of the estimation procedure setup (Figure 4B4) and it takes advantage of all the previous steps. Here, we used the constrained least squares technique to identify the parameters that best fit tube laws (2) and (22) to the observed in vitro data. Additionally, we fixed A_0 and p_0 to increase the identifiability of the remaining parameters, making the estimation process more accurate. We extracted the values of A_0 and p_0 in the averaged troughs (red cross in Figure 4B1) to ensure that these values were as precise as possible, given the minimal motion of the vessels at those points in the cycle. To provide an overview of the obtained results, Table 1 displays the values for A_0 and p_0 in terms of minimum, average and maximum for every type of vessel. The decision to fix A_0 and p_0 is based on two main reasons. Firstly, it is a common practice in hemodynamics to fix these parameters as A_0 and p_0 can be derived from experimental area-pressure data. Secondly, a local sensitivity and collinearity analysis (results not reported here)[35] showed that pressure $p(x,t)$ is very sensitive to changes in A_0. Therefore, we fixed it to avoid that the estimation problem was affected by inaccurate A_0 estimates.

The constrained least squares problem (Figure 4B4) reads

$$\text{Find } \mathbf{Z}\in\zeta \text{ such that } f(\mathbf{Z}) \text{ is minimized.} \tag{47}$$

$\mathbf{Z}$ is the vector representing the parameters to estimate. For the elastic tube law (2), $\mathbf{Z}=[K,m,n]$, while for the viscoelastic tube law (22), $\mathbf{Z}=[K,m,n,\Gamma]$. ζ is a subset of either $\mathbb{R}^3$ (elastic tube law) or $\mathbb{R}^4$ (viscoelastic tube law) representing the parameter space. $f(\mathbf{Z})$ is the objective function we need to minimize, whose expression is determined by the residual vector $\mathbf{r}(\mathbf{Z})$. Its i-th component is given by

$$r_i(\mathbf{Z}) = p_{exp}(t_i) - p_{approx}(\mathbf{Z};t_i), \tag{48}$$

where $p_{exp}(t)$ is the experimental area-pressure relation $\forall t \in \mathbb{R}^+$, obtained from the averaged experimental data (black curve in Figure 4B1), while $p_{approx}(\mathbf{Z};t)$ is the pressure curve that we want to parametrize and that must satisfy relation (2) or (22). We decided to evaluate the accuracy of the estimation process computing the root mean squared error (RMSE) between $p_{exp}(t)$ and $p_{approx}(\mathbf{Z};t)$, normalized with respect to the pressure range. Thus, the objective function reads

$$f(\mathbf{Z}) = \mathrm{RMSE} = \frac{\sqrt{\frac{1}{n_r}\sum_{i=1}^{n_r}(r_i(\mathbf{Z}))^2}}{\max\limits_{i=1,\dots,n_r}\left[p_{exp}(t_i)\right] - \min\limits_{i=1,\dots,n_r}\left[p_{exp}(t_i)\right]}, \tag{49}$$

where n_r is the size of $\mathbf{r}(\mathbf{Z})$. We solved the constrained least squares problem applying a constrained non-linear optimization technique, called Trust Region Reflective.[40,41] This method produces a solution only when the convergence conditions have been met. Specifically, we have implemented a termination tolerance for both cost function modification and change in independent variables, set at 10^{-15}.

We performed 4 estimations for each tube law (Table 2) using the described setup. For each estimation we performed 100 optimizations, defining each time a new random uniformly distributed initial guess, to ensure the convergence of the optimization process. Our aim was to compare the models, and investigate any differences between values of the parameters found in literature[6,11,12,32] and those obtained from our multiple estimations. Cases E1 and V1 are derived from constraints (45), while cases E4 and V4 come from constraints (46). Cases E2, E3, V2, and V3 are based on literature examples,[6,11,12,32] where m and n are fixed, and K and Γ are allowed to vary. The different cases define the subset ζ.

3 | RESULTS

Quantitative results are displayed in Figure 5 for each vessel type in terms of average (central dot), minimum (lower whisker) and maximum (upper whisker) RMSEs. The 5 panels on the left display the results for the estimations obtained using the elastic tube law (cases E1–E4), while the 5 panels on the right display the estimations for the viscoelastic tube law (cases V1–V4). Additionally, Table 3 reports the values assumed by the averaged RMSEs for the different vessel types and the different estimation cases.

Qualitative results are shown in Figures 6 and 7 in terms of fitted pressure curves (p_{approx}). These curves were derived by using the estimated parameters as input data for tube laws (2) and (22), in addition to the cross-sectional areas obtained from the experiments. Additionally, the time derivative in the viscoelastic tube law (22) has been discretized using the forward finite difference approximation. In each plot we have reported in black the considered experimental area-pressure curve, in blue the fitted pressure curve obtained with the elastic estimation cases E1–E4 and in red the fitted pressure curve obtained with the viscoelastic estimation cases V1–V4. The experimental area-pressure curve refer to HVCI for Figure 6 and to LVCI for Figure 7. Additionally, Figures A1–A3 of appendix show qualitative results for AA, LPA and Fem, respectively.

Finally, Figure 8 displays the values of the estimated parameters for six selected vessel types and for all the four viscoelastic estimation cases V1–V4, in terms of average (central dot), minimum (lower whisker) and maximum (upper whisker) values. The exact values of the average estimated parameters for case V1 and all vessel types are reported in Table 4. Whereas in appendix, Tables A1–A3 report the exact values of the averaged estimated parameters for estimation cases V2–V4, and Tables A4–A7 report the exact values of the averaged estimated parameters for estimation cases E1–E4.

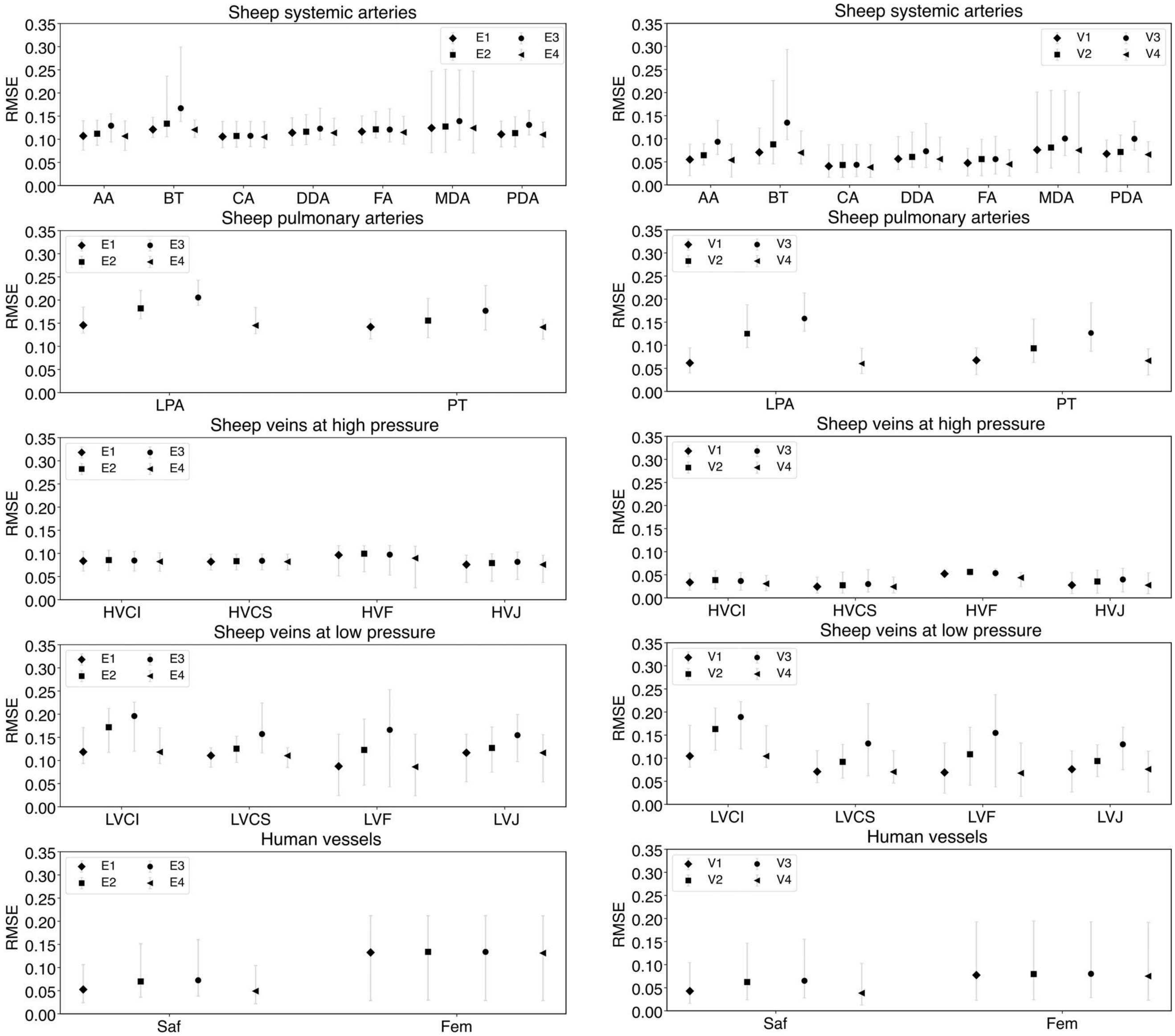

FIGURE 5 **RMSEs for all the vessel types and for both the elastic and the viscoelastic tube laws.** Average (central dot), minimum (lower whisker) and maximum (upper whisker) RMSEs for each vessel type. On the left, results of the four estimates with the elastic tube law (cases E1–E4). On the right, results of the four estimates with the viscoelastic tube law (cases V1–V4).

4 | DISCUSSION

4.1 | Accuracy

This section presents a comprehensive evaluation of the obtained results, with emphasis on accuracy and reliability of the parameter estimations made. After examining Figure 5 and Table 3, it becomes apparent that there is a noticeable pattern when comparing E1 to E4, as well as V1 to V4. These cases, which are based on constraints (45) and (46), demonstrate relatively similar average RMSEs for all types of vessels. This suggests that constraining m and n, as we did in E1 and V1 cases, has not a big impact on the accuracy of the estimations. The parameters consistently adopt the optimal configuration of values to achieve the lowest RMSE. More importantly, this aspect allowed us to verify the influence of constraints on estimations, particularly for the elastic tube law (2). Upon analyzing the results in Table A7, that report the obtained estimates of parameters for case E4, we can clearly observe that the estimates of n are always below -2 or above 0. This implies that constraints (45) are never met. Hence, the phenomenon we describe using parameters obtained from this fitting (case E4) might lead to the generation of waves that are not present in the cardiovascular

TABLE 3 Averaged RMSEs.

Vess.	Num.[a]	Averaged RMSE							
		E1	E2	E3	E4	V1	V2	V3	V4
Sheep systemic arteries									
AA	12	0.11	0.11	0.13	0.11	0.06	0.06	0.09	0.05
BT	11	0.12	0.13	0.17	0.12	0.07	0.09	0.13	0.07
CA	11	0.11	0.11	0.11	0.10	0.04	0.04	0.04	0.04
DDA	11	0.11	0.12	0.12	0.11	0.06	0.06	0.07	0.06
FA	11	0.12	0.12	0.12	0.11	0.05	0.06	0.06	0.04
MDA	11	0.12	0.13	0.14	0.12	0.08	0.08	0.10	0.08
PDA	11	0.11	0.11	0.13	0.11	0.07	0.07	0.10	0.07
Sheep pulmonary arteries									
LPA	11	0.15	0.18	0.21	0.15	0.06	0.13	0.16	0.06
PT	10	0.14	0.16	0.18	0.14	0.07	0.09	0.13	0.07
Sheep veins at high (H) pressure									
HVCI	5	0.08	0.09	0.08	0.08	0.03	0.04	0.04	0.03
HVCS	8	0.08	0.08	0.08	0.08	0.02	0.03	0.03	0.02
HVF	5	0.10	0.10	0.10	0.09	0.05	0.06	0.05	0.04
HVJ	8	0.08	0.08	0.08	0.08	0.03	0.04	0.04	0.03
Sheep veins at low (L) pressure									
LVCI	10	0.12	0.17	0.20	0.12	0.10	0.16	0.19	0.10
LVCS	12	0.11	0.13	0.16	0.11	0.07	0.09	0.13	0.07
LVF	30	0.09	0.12	0.17	0.09	0.07	0.11	0.15	0.07
LVJ	10	0.12	0.13	0.15	0.12	0.08	0.09	0.13	0.08
Human vessels									
Fem	30	0.13	0.13	0.13	0.13	0.08	0.08	0.08	0.08
Saf	20	0.05	0.07	0.07	0.05	0.04	0.06	0.07	0.04

Note: Averaged RMSEs for all the estimation cases (E1–E4 and V1–V4) and for all the vessel types (Vess.).
[a]Number of available sets of data for each type of vessel.

system. It is evident that while constraining m and n is not essential when dealing with the viscoelastic tube law (23), it is crucial when we use the elastic tube law (2).

Our results (see Figure 5 and Table 3) show also that average RMSEs for cases E2, E3 and V2, V3 are higher compared to those for cases E1, E4, and V1, V4. By allowing for estimation of m and n in a tube law (cases E1, E4, and V1, V4), we enhance the precision of the parameter estimation. The greater weight of uncertainty and errors in cases E2, E3, and V2, V3 is due to the limited number of adjustable parameters (K and Γ) in these cases. Conversely, in cases E1, E4, and V1, V4, all parameters can vary freely and reach the optimal configuration, resulting in smaller RMSEs. Additionally, the cases that present the highest errors are always E3 and V3. Therefore, if m and n cannot be estimated, but they have to be fixed, then values $m = 10.0$ and $n = -1.5$ (E2 and V2 cases) should be used instead of $m = 0.5$ and $n = 0.0$ (E3 and V3 cases).

Finally, if we compare average RMSEs for elastic cases E1–E4 (Figure 5 left panels) with average RMSEs for viscoelastic cases V1–V4 (Figure 5 right panels), for all the vessel types, we observe that average RMSEs for the viscoelastic cases are lower than those of the elastic cases. Therefore viscoelasticity cannot be neglected and the viscoelastic tube law should be used instead of the elastic tube law, whenever possible.

Studying now qualitative results, if we compare Figure 6A (7A) with Figure 6D (7D), namely the curves obtained considering cases E1 (V1) and E4 (V4), we cannot see any clear distinction among them. This is in agreement with the previous results, where we showed that averaged RMSEs for these cases are similar. Although the pressure curves fitted

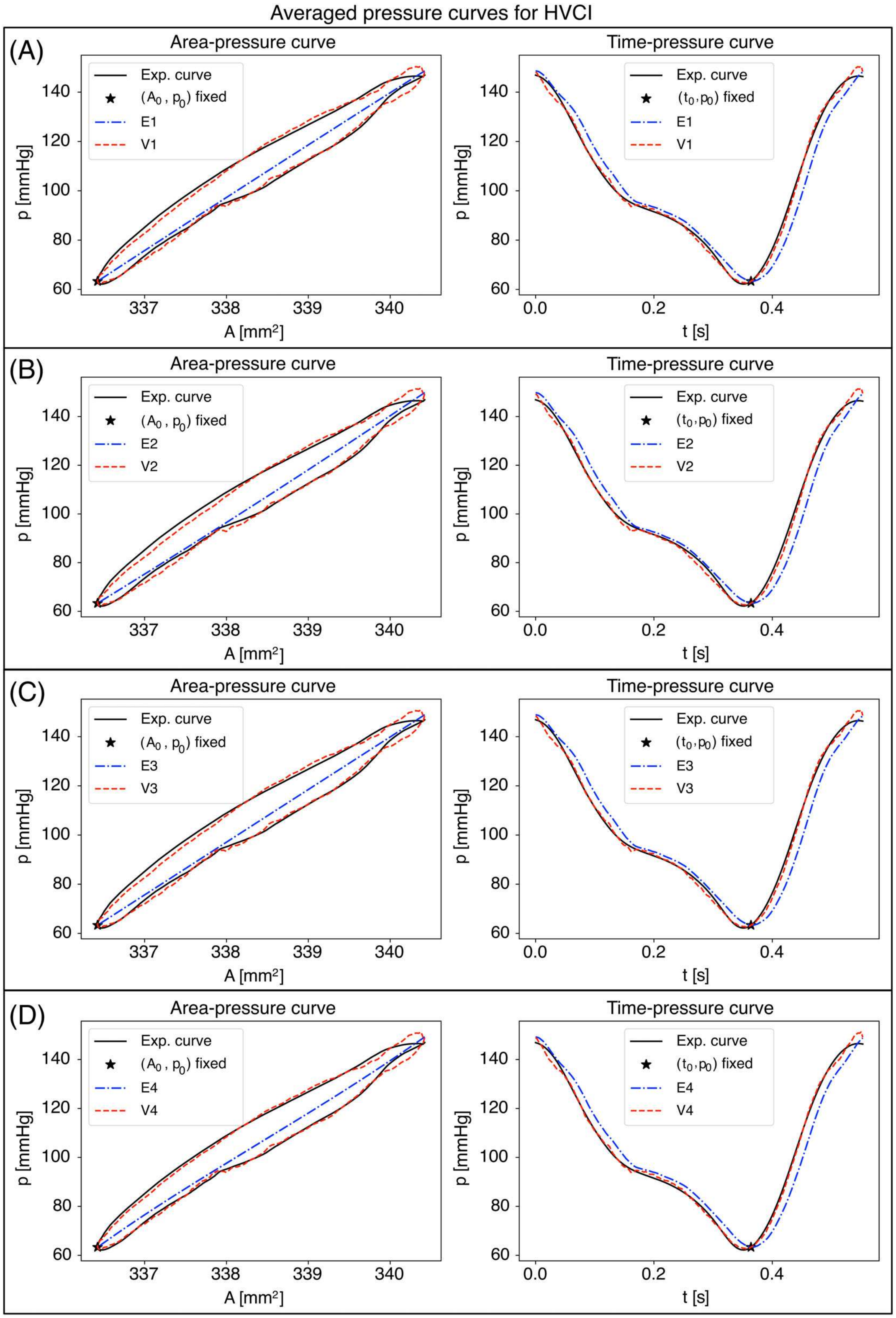

FIGURE 6 Fitted pressure curves for HVCI. Comparison between experimental and fitted pressure curves for all the estimation cases of an example dataset of VCI at high (H) pressure. Black solid lines represent averaged experimental area-pressure and time–pressure curves, blue dash-dot lines represent the fitted curves obtained considering the elastic cases E1–E4, while red dashed lines represent the fitted curves obtain considering the viscoelastic cases V1–V4.

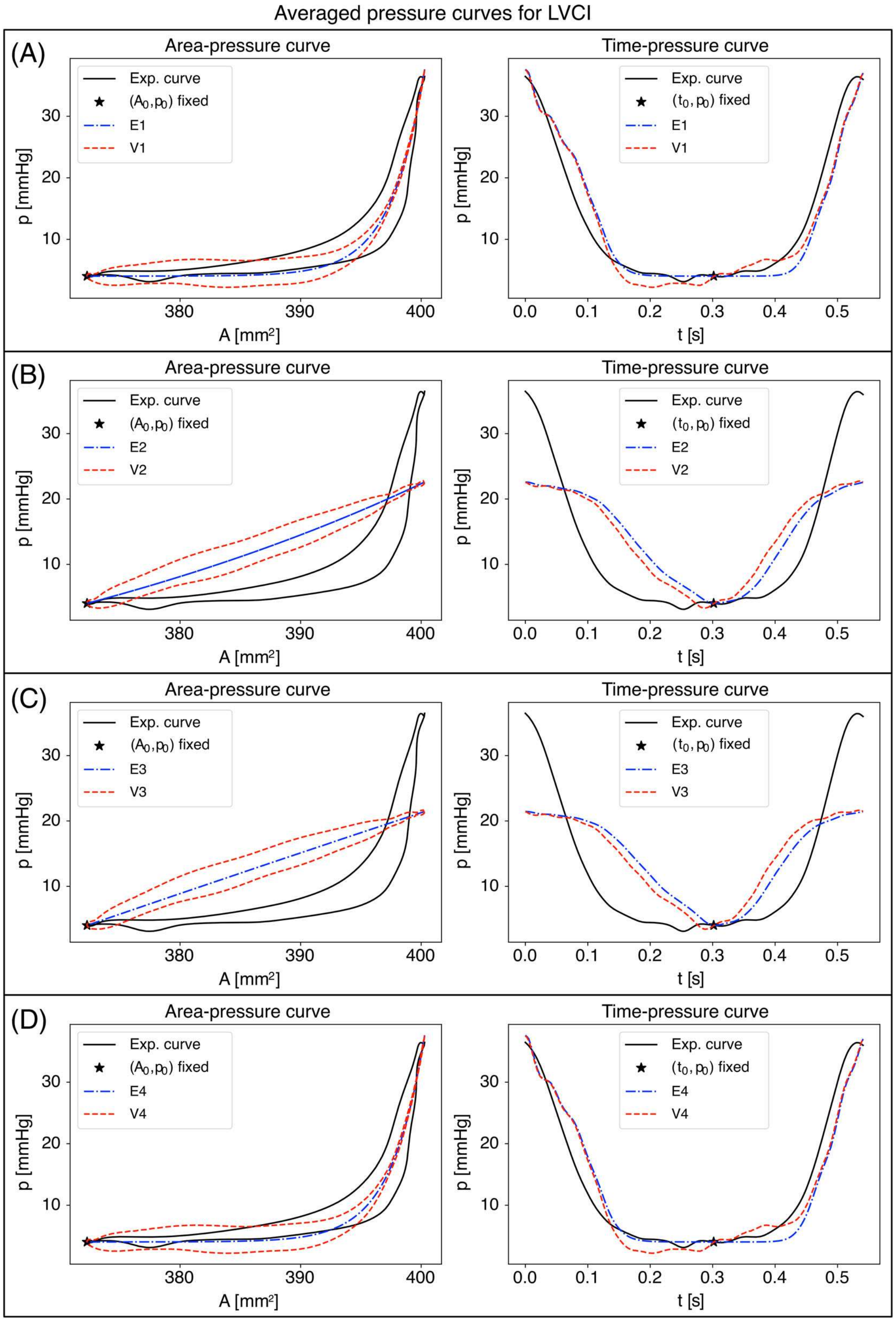

FIGURE 7 **Fitted pressure curves for LVCI.** Comparison between experimental and fitted pressure curves for all the estimation cases of an example dataset of VCI at low (L) pressure. Black solid lines represent averaged experimental area-pressure and time–pressure curves, blue dash-dot lines represent the fitted curves obtained considering the elastic cases E1–E4, while red dashed lines represent the fitted curves obtain considering the viscoelastic cases V1–V4.

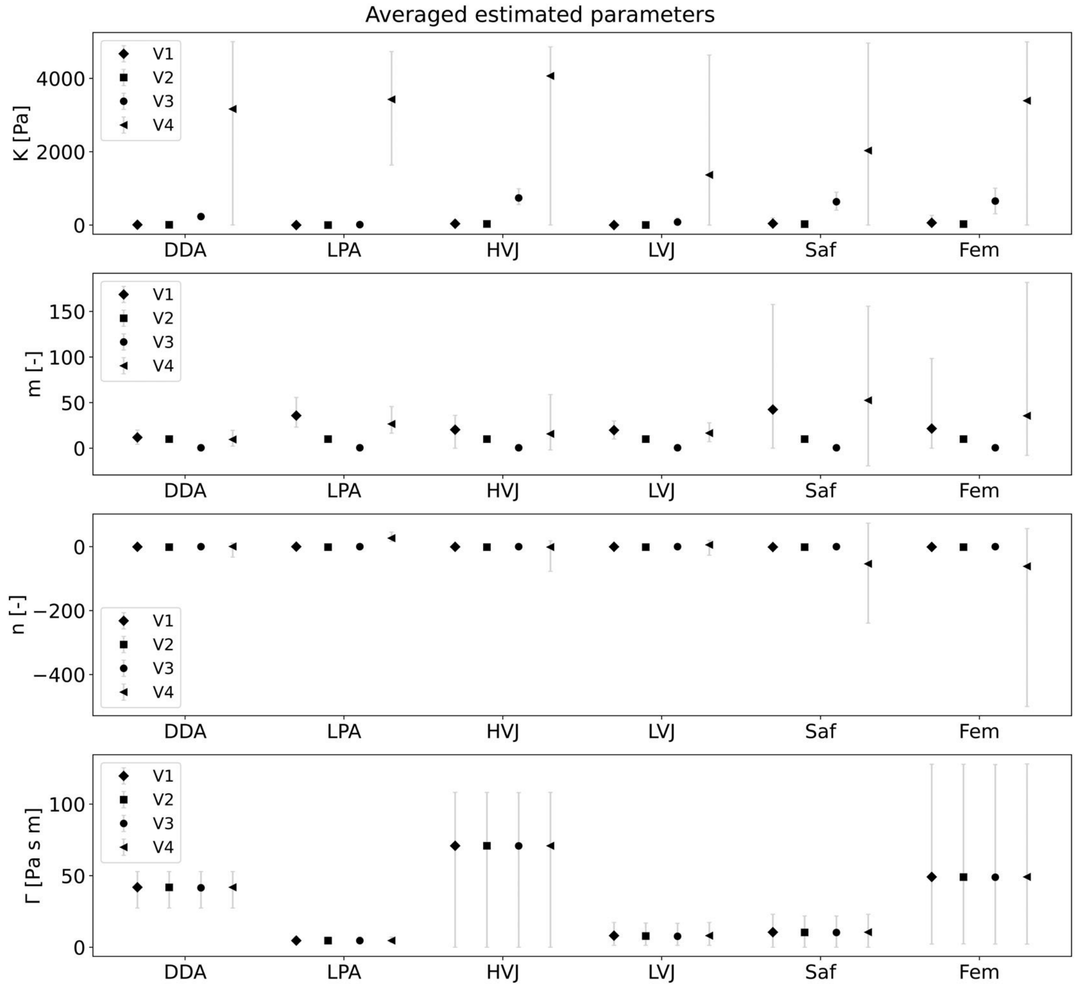

FIGURE 8 Averaged estimated parameters of the viscoelastic tube law. Averaged (central dot), minimum (lower whisker) and maximum (upper whisker) estimated parameters of the viscoelastic tube law for six selected vessel types and for all the viscoelastic estimation cases V1–V4.

for case E4 showed in Figures 6D and 7D resemble the experimental pressure curves, it is important to note that this outcome may not be replicated in more complex vessel networks. Instead, when comparing panels (A) and (D) with panels (B) and (C), it is evident that the fitted pressure curves obtained from cases E1, E4, and V1, V4 (with m and n allowed to vary) better approximate the experimental area-pressure curves, particularly in the case of LVCI (Figure 7). By fixing m and n in cases E2, E3, and V2, V3, we limit the ability to capture the non-linearity of the curve to only K and Γ. If all four parameters are allowed to change, as expected a better fit can be found. This scenario corresponds to what we have underlined previously in terms of averaged RMSEs, even though the differences between E2 (V2) and E3 (V3) cases are not qualitatively detectable. The pressure curves in panels (B) and (C) of both Figures 6 and 7 are very similar.

Finally, if we look at Figures 6 and 7, it is clear that the hysteresis cycles are better captured by the red dashed lines, which are the fitted curves obtained using the viscoelastic tube law. The agreement between these curves and the experimental area-pressure curves is satisfactory, especially in V1 and V4 cases. Instead the blue lines, which represent the fitted curves obtained with the elastic tube law, approximate the hysteresis with straight lines and slightly overestimate the pressure peaks in the pressure–time curves. These final considerations are significant because they confirm again our quantitative results and because similar observations have been made also by other authors.[4,16]

Before proceeding further, a remark has to be made. Among all the datasets that we used for this study, we observed that some of them present averaged experimental area-pressure curves with squeezed or twisted hysteresis cycles. Despite the particular shape of these averaged experimental data, the estimation process was only slightly affected. The obtained RMSEs for these particular datasets all belong to the upper whiskers (Figure 5) of the vessel types the datasets

TABLE 4 Averaged estimated parameters of the viscoelastic tube law for V1 estimation case.

Vess.	Num.[a]	K [kPa]	m [−]	n [−]	Γ [Pa s m]
Sheep systemic arteries					
AA	12	1.78	8.31	−0.83	13.69
BT	11	1.13	14.80	−1.27	19.26
CA	11	202.74	14.21	−1.27	93.89
DDA	11	8.68	11.85	−0.55	41.89
FA	11	40.16	9.30	−0.91	22.61
MDA	11	4.27	8.67	−1.36	19.66
PDA	11	2.02	10.96	−1.64	16.01
Sheep pulmonary arteries					
LPA	11	0.02	35.78	−0.00	4.66
PT	10	0.13	20.85	−0.00	4.86
Sheep veins at high (H) pressure					
HVCI	5	274.83	7.98	−1.60	214.50
HVCS	8	88.23	14.25	−0.25	140.46
HVF	5	97.18	6.22	−2.00	28.44
HVJ	8	36.47	20.31	−0.50	70.88
Sheep veins at low (L) pressure					
LVCI	10	19.29	64.22	−0.80	7.04
LVCS	12	0.75	15.34	−1.33	8.70
LVF	30	3.45	21.54	−0.87	4.16
LVJ	10	0.65	19.78	−0.40	8.09
Human vessels					
Fem	30	62.07	21.54	−0.93	49.12
Saf	20	41.73	42.41	−1.20	10.52

[a]Number of available sets of data for each type of vessel.

refer to. However, they never assume the maximum RMSE value. Therefore, we decided to maintain these datasets as part of the study. Nevertheless, it means that the tube laws we are considering are not able to reproduce this kind of waveforms. A more sophisticated tube law that encompasses additional physical factors should be examined, such as the tube laws utilized in Bertaglia et al.[14] or in Valdez-Jasso et al.[19]

4.2 | Averaged estimated parameters

The ability of the viscoelastic tube law (22) to better approximate the behavior of the experimental area-pressure relations has been demonstrated in the previous section, where quantitative and qualitative comparisons between elastic and viscoelastic models have been made. Nevertheless, the elastic tube law is still widely used, thanks to its simpler formulation and its good representation of the dominating effect, the elastic response to vessel wall's deformations. However, predictably, when modeling hysteresis cycles, viscoelasticity is crucial. This is also confirmed by the averaged estimated parameters obtained with the viscoelastic tube law. If we examine the last panel in Figure 8, which shows the results obtained for the viscoelasticity parameter Γ, it is worth noting that the average estimates across all cases and those specific to individual vessel types are nearly indistinguishable, despite the variability of the estimates of the different datasets of a specific vessel type can be significant. This observation is confirmed by results reported in Tables 4 and A1–A3, which clearly show that Γ values for individual vessel types are very similar. This indicates that Γ is distinct for a specific vessel type and can be accurately estimated. Additionally, if we study the differences between vessel types, we observe how Γ estimated values have an order of magnitude of difference between pulmonary and systemic arteries.

Our results show that the viscoelasticity of LPA and PT is lower than the viscoelasticity of the systemic arteries and assume a value around 4.76 Pa s m. Conversely, systemic arteries range between 13.69 and 93.89 Pa s m, with an increase in Γ from AA towards DDA. This is in agreement with the observations made by Bia et al,[9] where the authors showed that the increase in the viscoelasticity depends on the amounts of collagen and smooth muscle cells, components of the vessel walls.[10,31] As for the ovine veins, rather different values of Γ have been obtained for the same type of veins at low and high pressure. Particularly, results for data regarding high pressure veins produced a viscoelasticity coefficient that is at least one order of magnitude greater than low pressure veins. This is in agreement with different studies,[20] where it has been observed that veins viscoelasticity has the functional role of energy dissipation and adaptive response to hemodynamic overload conditions.

Observing now the panels for K, m and n parameters of Figure 8, we see that the values of the three parameters can change and modify themselves to always have the best approximation of the experimental data. Nevertheless, analyzing Tables 4 and A3, we note how the estimated values of the stiffness coefficient K increase from AA towards DDA. Different studies on arterial wall composition[9] show that the quantity of elastin directly influences arterial wall compliance and that there is an increase in compliance from peripheral arteries to the aortic root, thus the increase we observed in K aligns with such physiological observations. Moreover, we observe that the values of K are higher for muscular arteries, such as the peripheral arteries CA and FA, compared to other ovine arteries. This is noteworthy as K is proportional to the Young's elastic modulus, to the vessel wall thickness and to the inverse of the vessel radius.[4] Thus, since CA and FA have smaller diameters respect the other considered arteries, the small radius can lead to higher values of K in these two cases. The higher values of CA and FA are also coherent with the fact that external vessels have thicker walls than inner vessels because they must be able to resist also to external forces that could deform them.[31] Instead, ovine veins exhibit even higher estimated values of K compared to arteries. But in this case the explanation of high values is connected with the presence of collagen. Veins indeed are more compliant at low pressure values than arteries, but for high pressures they become very stiff.[20]

Regarding the other two parameters (m and n), central panels of Figure 8 show that the obtained averaged estimated m and n for cases V1 and V4 differ from the literature values that we were considering (V2, V3 cases). Specifically, it can be read in Tables 4 and A3 how all the estimated values of m range between 6.22 and 64.22, and this is in line with the fact that for $m > 1$ vessels tend to become stiffer as deformations grow, as it happens for real vessels. When a value of $m < 1$ is assumed, the described behavior is the opposite. Vessels tend to be softer for high pressure values, but this is against physiological observations. Thus, this is a further confirmation that case V3 ($m = 0.5$ and $n = 0.0$) and in general any value of $m < 1$, should not be adopted if large vessel deformations are to be modeled.

5 | CONCLUSION

In this work, we estimated the parameters of elastic and viscoelastic tube laws using in vitro data from ovine and human sources. Our methodology involved constraining the parameters to specific ranges in order to maintain prescribed mathematical properties.

The results we obtained demonstrate that both the elastic and the viscoelastic tube laws can replicate the in vitro experimental data. Nevertheless, we noted that the elastic tube law cannot depict the experimentally observed hysteresis cycles owing to the absence of the viscous term in its formulation. Furthermore, it has been noted that the viscoelastic tube law provides a quantitative and qualitative description of all in vitro data utilized in this study. However, the law's viscous component requires improvement to represent more tightly or twisted hysteresis cycles effectively. A dependency on pressure, similar to the one proposed in Bertaglia et al.,[14] should be included to achieve better capture of these particular hysteresis cycles.

Within this study, it was demonstrated that the constraining procedure is essential for obtaining accurate estimates that can be utilized in more complex blood vessel networks, particularly when considering the elastic tube law. The calibrated models are appropriate for representing the pressure-area relationship under experimentally observed pressure conditions. If specific phenomena, such as vessels' collapse or stiffening, need to be described, new parameterizations of the tube laws are necessary. In fact, the tube laws we are currently considering are incomplete. Proper generalization of both low and high-pressure regimes can be achieved simultaneously by adding new non-linear terms to the mathematical formulation of the tube laws or by coupling the models we are considering with other specific models to describe the particular phenomena.

Finally, we also tested the two tube laws by allowing all their parameters to vary freely within their respective ranges and by fixing some of their parameters. We observed that it is desirable to adopt the first approach ("leaving the parameters free") to ensure that the experimental pressure-area curves are reproduced adequately. Nevertheless, we also observed that anyhow it is possible to fix some of the parameters of the tube laws, but careful consideration must be given to the chosen values.

ACKNOWLEDGMENTS

The first and second authors acknowledge the Italian Ministry of Education, Universities and Research (MUR), in the framework of the project DICAM-EXC (Departments of Excellence 2023-2027, grant L232/2016).

CONFLICT OF INTEREST STATEMENT

The authors declare no conflict of interest.

DATA AVAILABILITY STATEMENT

Research data are not shared.

ORCID

Chiara Colombo https://orcid.org/0009-0004-6886-5219
Annunziato Siviglia https://orcid.org/0000-0003-1192-1596
Daniel Bia https://orcid.org/0000-0001-7160-7166
Yanina Zócalo https://orcid.org/0000-0002-6544-2518
Lucas O. Müller https://orcid.org/0000-0003-1933-8995

REFERENCES

1. Formaggia L, Quarteroni A, Veneziani A. Cardiovascular mathematics. *Modeling and Simulation of the Circulatory System*. Springer; 2009.
2. Liang F, Guan D, Alastruey J. Determinant factors for arterial hemodynamics in hypertension: theoretical insights from a computational model-based study. *J Biomech Eng*. 2018;140(3):1.
3. Mynard JP, Smolich JJ. One-dimensional haemodynamic modeling and wave dynamics in the entire adult circulation. *Ann Biomed Eng*. 2015;43(6):1443-1460.
4. Alastruey J, Khir AW, Matthys KS, et al. Pulse wave propagation in a model human arterial network: assessment of 1-d visco-elastic simulations against in vitro measurements. *J Biomech*. 2011;44(12):2250-2258.
5. Boileau E, Nithiarasu P, Blanco PJ, et al. A benchmark study of numerical schemes for one-dimensional arterial blood flow modelling. *Int J Num Meth Biomed Eng*. 2015;31:e02732.
6. Müller LO, Toro EF. A global multiscale mathematical model for the human circulation with emphasis on the venous system. *Int J Numer Methods Biomed Eng*. 2014;30(7):681-725.
7. Reymond P, Merenda F, Perren F, Rüfenacht D, Stergiopulos N. Validation of a one-dimensional model of the systemic arterial tree. *Am J Physiol Heart Circ Physiol*. 2009;297(1):H208-H222.
8. Xiao N, Alastruey J, Figueroa C. A systematic comparison between 1-D and 3-D hemodynamics in compliant arterial models. *Int J Num Meth Biomed Eng*. 2014;30:204-231.
9. Bia D, Zócalo Y, Cabrera-Fischer EI, Wray S, Armentano RL. Quantitative analysis of the relationship between blood vessel wall constituents and viscoelastic properties: dynamic biomechanical and structural in vitro studies in aorta and carotid arteries. *Phys J*. 2014;2014:142421.
10. Burton AC. Relation of structure to function of the tissues of the wall of blood vessels. *Physiol Rev*. 1954;34(4):619-642.
11. Formaggia L, Lamponi D, Quarteroni A. One-dimensional models for blood flow in arteries. *J Eng Math*. 2003;47(3):251-276.
12. Brook BS, Falle SAEG, Pedley TJ. Numerical solutions for unsteady gravity-driven flows in collapsible tubes: evolution and roll-wave instability of a steady state. *J Fluid Mech*. 1999;396:223-256.
13. Pedley TJ, Brook BS, Seymour RS. Blood pressure and flow rate in the giraffe jugular vein. *Philos Trans R Soc London Ser B*. 1996;351(1342):855-866.
14. Bertaglia G, Caleffi V, Valiani A. Modeling blood flow in viscoelastic vessels: the 1d augmented fluid–structure interaction system. *Comput Methods Appl Mech Eng*. 2020;360:112772.
15. Müller LO, Blanco PJ, Watanabe SM, Feijóo RA. A high-order local time stepping finite volume solver for one-dimensional blood flow simulations: application to the adan model. *Int J Numer Methods Biomed Eng*. 2016;32(10):e02761.
16. Battista C, Bia D, Germán YZ, Armentano RL, Haider MA, Olufsen MS. Wave propagation in a 1d fluid dynamics model using pressure-area measurements from ovine arteries. *J Mech Med Biol*. 2016;16(2):1650007.

17. Quarteroni A, Tuveri M, Veneziani A. Computational vascular fluid dynamics: problems, models and methods. *Comput Vis Sci*. 2000;2: 163-197.
18. Bia Santana D, Armentano RL, Zócalo Y, et al. Functional properties of fresh and cryopreserved carotid and femoral arteries, and of venous and synthetic grafts: comparison with arteries from normotensive and hypertensive patients. *Cell tissue banking*. 2007;8(1):43-57.
19. Valdez-Jasso D, Bia D, Zócalo Y, Armentano RL, Haider MA, Olufsen MS. Linear and nonlinear viscoelastic modeling of aorta and carotid pressure–area dynamics under in vivo and ex vivo conditions. *Ann Biomed Eng*. 2011;39(5):1438-1456.
20. Zócalo Y, Bia D, Cabrera-Fischer EI, Wray S, Galli C, Armentano RL. Structural and functional properties of venous wall: relationship between elastin, collagen, and smooth muscle components and viscoelastic properties. *ISRN Physiol*. 2013;2013:906031.
21. Spilimbergo A, Toro EF, Müller LO. One-dimensional blood flow with discontinuous properties and transport: mathematical analysis and numerical schemes. *Commun Comput Phys*. 2021;29(3):649-697.
22. Toro EF, Siviglia A. Flow in collapsible tubes with discontinuous mechanical properties: mathematical model and exact solutions. *Commun Comput Phys*. 2013;13(2):361-385.
23. Toro EF. *Riemann Solvers and Numerical Methods for Fluid Dynamics*. Springer; 2009.
24. Flores J, Alastuey J, Corvera Poiré E. A novel analytical approach to pulsatile blood flow in the arterial network. *Ann Biomed Eng*. 2016; 44(10):3047-3068.
25. Sazonov I, Nithiarasu P. A novel, FFT-based one-dimensional blood flow solution method for arterial network. *Biomech Model Mechanobiol*. 2019;18:1311-1334.
26. Quarteroni A. *Modellistica numerica per problemi differenziali*. Springer; 2012.
27. Cattaneo C. A form of heat-conduction equations which eliminates the paradox of instantaneous propagation. *CR Acad Sci*. 1958; 247:431.
28. Montecinos GI, Müller LO, Toro EF. Hyperbolic reformulation of a 1d viscoelastic blood flow model and ader finite volume schemes. *J Comput Phys*. 2014;266:101-123.
29. Montecinos GI, Toro EF. Reformulations for general advection–diffusion–reaction equations and locally implicit ader schemes. *J Comput Phys*. 2014;275:415-442.
30. Bressan A. *Hyperbolic Systems of Conservation Laws: the One-Dimensional Cauchy Problem*. Oxford University Press; 2000.
31. Levick JR. *An Introduction to Cardiovascular Physiology*. Hodder Arnold; 2009.
32. Siviglia A, Toffolon M. Steady analysis of transcritical flows in collapsible tubes with discontinuous mechanical properties: implications for arteries and veins. *J Fluid Mech*. 2013;736:195-215.
33. Caro CG, Pedley TJ, Schroter RC, Seed WA. *The Mechanics of the Circulation*. Cambridge university press; 2012.
34. Fung YC. *Biomechanics*. Springer; 1997.
35. Colombo C. *Mathematical Properties-Preserving Parameter Estimation for a Blood Flow Model Using Ovine and Human In Vitro Data*. University of Trento; 2021.
36. Caníc S, Tambaca J, Guidoboni G, Mikelíc A, Hartley CJ, Rosenstrauch D. Modeling viscoelastic behavior of arterial walls and their interaction with pulsatile blood flow. *SIAM J Appl Math*. 2006;67(1):164-193.
37. Zócalo Y, Bia D, Pessana FM, Armentano RL. Changes in vein dynamics ranging from low to high pressure levels as a determinant of the differences in vein adaptation to arterial hemodynamic conditions. *Artif Organs*. 2007;31(7):575-580.
38. United States Naval Reserve Council. *Guide for the Care and Use of Laboratory Animals*. Washington, DC. National Academy Press; 1996.
39. Bia D, Zócalo Y, Armentano RL, Camús J, de Forteza E, Cabrera-Fischer E. The adventitia reduces left ventricular dynamic afterload via smooth muscle activation-dependent mechanisms. *Rev Esp Cardiol*. 2007;60(5):501-509.
40. Branch MA, Coleman TF, Li Y. A subspace, interior, and conjugate gradient method for large-scale bound-constrained minimization problems. *SIAM J Sci Comput*. 1999;21(1):1-23.
41. Nocedal J, Wright SJ. Numerical optimization. *And S*. Springer; 1999.

How to cite this article: Colombo C, Siviglia A, Toro EF, Bia D, Zócalo Y, Müller LO. Tube law parametrization using in vitro data for one-dimensional blood flow in arteries and veins. *Int J Numer Meth Biomed Engng*. 2024;40(4):e3803. doi:10.1002/cnm.3803

APPENDIX A

TABLE A1 Averaged estimated parameters of the viscoelastic tube law for V2 estimation case.

Vess.	Num.[a]	K [kPa]	m [−]	n [−]	Γ [Pa s m]
Sheep systemic arteries					
AA	12	1.04	10.00	−1.50	13.75
BT	11	1.90	10.00	−1.50	18.96
CA	11	46.23	10.00	−1.50	93.91
DDA	11	7.78	10.00	−1.50	41.83
FA	11	11.25	10.00	−1.50	22.63
MDA	11	2.48	10.00	−1.50	19.72
PDA	11	2.01	10.00	−1.50	15.98
Sheep pulmonary arteries					
LPA	11	0.35	10.00	−1.50	4.63
PT	10	0.31	10.00	−1.50	4.82
Sheep veins at high (H) pressure					
HVCI	5	60.10	10.00	−1.50	214.30
HVCS	8	38.96	10.00	−1.50	140.23
HVF	5	22.62	10.00	−1.50	28.46
HVJ	8	30.38	10.00	−1.50	70.87
Sheep veins at low (L) pressure					
LVCI	10	7.26	10.00	−1.50	6.85
LVCS	12	1.73	10.00	−1.50	8.61
LVF	30	5.10	10.00	−1.50	4.12
LVJ	10	2.45	10.00	−1.50	7.84
Human vessels					
Fem	30	27.00	10.00	−1.50	49.02
Saf	20	26.19	10.00	−1.50	10.36

[a]Number of available sets of data for each type of vessel.

TABLE A2 Averaged estimated parameters of the viscoelastic tube law for V3 estimation case.

Vess.	Num.[a]	K [kPa]	m [−]	n [−]	Γ [Pa s m]
Sheep systemic arteries					
AA	12	61.73	0.50	0.00	13.25
BT	11	77.13	0.50	0.00	18.55
CA	11	1118.40	0.50	0.00	93.83
DDA	11	231.43	0.50	0.00	41.53
FA	11	309.42	0.50	0.00	22.57
MDA	11	104.99	0.50	0.00	19.29
PDA	11	90.48	0.50	0.00	15.55
Sheep pulmonary arteries					
LPA	11	12.33	0.50	0.00	4.62
PT	10	11.34	0.50	0.00	4.80
Sheep veins at high (H) pressure					
HVCI	5	1443.86	0.50	0.00	214.01
HVCS	8	954.26	0.50	0.00	139.84
HVF	5	566.34	0.50	0.00	28.41
HVJ	8	739.41	0.50	0.00	70.80
Sheep veins at low (L) pressure					
LVCI	10	186.58	0.50	0.00	6.74
LVCS	12	60.95	0.50	0.00	8.49
LVF	30	134.18	0.50	0.00	4.07
LVJ	10	82.20	0.50	0.00	7.65
Human vessels					
Fem	30	654.62	0.50	0.00	48.91
Saf	20	636.63	0.50	0.00	10.30

[a]Number of available sets of data for each type of vessel.

TABLE A3 Averaged estimated parameters of the viscoelastic tube law for V4 estimation case.

Vess.	Num.[a]	K [kPa]	m [−]	n [−]	Γ [Pa s m]
Sheep systemic arteries					
AA	12	2107.74	7.37	−7.24	13.69
BT	11	1656.61	13.24	−5.01	19.24
CA	11	1642.17	50.06	−119.39	93.80
DDA	11	3165.27	9.62	0.52	41.89
FA	11	2709.82	13.85	−29.50	22.58
MDA	11	1309.26	9.89	−18.53	19.70
PDA	11	857.79	12.47	−19.24	16.07
Sheep pulmonary arteries					
LPA	11	3426.68	26.59	26.59	4.66
PT	10	3779.99	14.26	14.26	4.86
Sheep veins at high (H) pressure					
HVCI	5	2708.33	20.35	−49.90	214.15
HVCS	8	3932.77	12.38	−1.06	140.48
HVF	5	866.30	36.36	−128.80	28.39
HVJ	8	4066.46	15.74	−1.30	70.86
Sheep veins at low (L) pressure					
LVCI	10	2906.49	53.66	−10.16	7.04
LVCS	12	1042.70	14.71	−15.95	8.70
LVF	30	2074.47	20.11	−61.35	4.17
LVJ	10	1367.72	16.60	5.65	8.08
Human vessels					
Fem	30	3390.90	35.58	−61.58	49.14
Saf	20	2030.91	52.48	−53.74	10.50

[a]Number of available sets of data for each type of vessel.

TABLE A4 Averaged estimated parameters of the elastic tube law for E1 estimation case.

Vess.	Num.[a]	K [kPa]	m [−]	n [−]	Γ [Pa s m]
Sheep systemic arteries					
AA	12	1.92	7.94	−0.71	0.00
BT	11	1.18	14.46	−1.09	0.00
CA	11	231.98	13.89	−1.48	0.00
DDA	11	9.88	11.14	−0.18	0.00
FA	11	43.01	8.95	−0.91	0.00
MDA	11	5.09	8.14	−1.09	0.00
PDA	11	2.19	10.56	−1.64	0.00
Sheep pulmonary arteries					
LPA	11	0.02	35.74	0.00	0.00
PT	10	0.13	20.56	0.00	0.00
Sheep veins at high (H) pressure					
HVCI	5	274.17	7.53	−1.60	0.00
HVCS	8	90.53	12.92	−0.25	0.00
HVF	5	97.90	5.58	−2.00	0.00
HVJ	8	38.02	20.02	−0.50	0.00
Sheep veins at low (L) pressure					
LVCI	10	19.30	64.05	−0.80	0.00
LVCS	12	0.93	14.78	−1.33	0.00
LVF	30	3.96	21.19	−0.80	0.00
LVJ	10	0.73	18.69	−0.40	0.00
Human vessels					
Fem	30	79.48	18.04	−0.97	0.00
Saf	20	41.94	42.13	−1.20	0.00

[a]Number of available sets of data for each type of vessel.

TABLE A5 Averaged estimated parameters of the elastic tube law for E2 estimation case.

Vess.	Num.[a]	K [kPa]	m [−]	n [−]	Γ [Pa s m]
Sheep systemic arteries					
AA	12	1.03	10.00	−1.50	0.00
BT	11	1.88	10.00	−1.50	0.00
CA	11	46.13	10.00	−1.50	0.00
DDA	11	7.74	10.00	−1.50	0.00
FA	11	11.21	10.00	−1.50	0.00
MDA	11	2.46	10.00	−1.50	0.00
PDA	11	1.99	10.00	−1.50	0.00
Sheep pulmonary arteries					
LPA	11	0.35	10.00	−1.50	0.00
PT	10	0.31	10.00	−1.50	0.00
Sheep veins at high (H) pressure					
HVCI	5	59.90	10.00	−1.50	0.00
HVCS	8	38.87	10.00	−1.50	0.00
HVF	5	22.56	10.00	−1.50	0.00
HVJ	8	30.29	10.00	−1.50	0.00
Sheep veins at low (L) pressure					
LVCI	10	7.25	10.00	−1.50	0.00
LVCS	12	1.70	10.00	−1.50	0.00
LVF	30	5.09	10.00	−1.50	0.00
LVJ	10	2.42	10.00	−1.50	0.00
Human vessels					
Fem	30	26.79	10.00	−1.50	0.00
Saf	20	26.17	10.00	−1.50	0.00

[a]Number of available sets of data for each type of vessel.

TABLE A6 Averaged estimated parameters of the elastic tube law for E3 estimation case.

Vess.	Num.[a]	*K* [kPa]	*m* [−]	*n* [−]	Γ [Pa s m]
Sheep systemic arteries					
AA	12	61.36	0.50	0.00	0.00
BT	11	76.75	0.50	0.00	0.00
CA	11	1116.08	0.50	0.00	0.00
DDA	11	230.46	0.50	0.00	0.00
FA	11	308.58	0.50	0.00	0.00
MDA	11	104.32	0.50	0.00	0.00
PDA	11	89.98	0.50	0.00	0.00
Sheep pulmonary arteries					
LPA	11	12.29	0.50	0.00	0.00
PT	10	11.31	0.50	0.00	0.00
Sheep veins at high (H) pressure					
HVCI	5	1439.15	0.50	0.00	0.00
HVCS	8	951.97	0.50	0.00	0.00
HVF	5	564.91	0.50	0.00	0.00
HVJ	8	737.28	0.50	0.00	0.00
Sheep veins at low (L) pressure					
LVCI	10	186.43	0.50	0.00	0.00
LVCS	12	60.23	0.50	0.00	0.00
LVF	30	133.82	0.50	0.00	0.00
LVJ	10	81.41	0.50	0.00	0.00
Human vessels					
Fem	30	649.82	0.50	0.00	0.00
Saf	20	636.01	0.50	0.00	0.00

[a]Number of available sets of data for each type of vessel.

TABLE A7 Averaged estimated parameters of the elastic tube law for E4 estimation case.

Vess.	Num.[a]	K [kPa]	m [−]	n [−]	Γ [Pa s m]
Sheep systemic arteries					
AA	12	2697.51	6.85	−7.11	0.00
BT	11	2242.90	12.31	−2.30	0.00
CA	11	1613.42	46.08	−118.27	0.00
DDA	11	4071.37	7.57	2.69	0.00
FA	11	2720.88	13.43	−28.23	0.00
MDA	11	1768.51	9.13	−15.11	0.00
PDA	11	869.77	12.00	−15.81	0.00
Sheep pulmonary arteries					
LPA	11	2982.01	26.56	26.56	0.00
PT	10	4031.61	14.02	14.02	0.00
Sheep veins at high (H) pressure					
HVCI	5	2789.18	18.67	−51.56	0.00
HVCS	8	3984.47	11.20	−0.40	0.00
HVF	5	834.91	35.58	−128.05	0.00
HVJ	8	3879.75	15.59	−2.21	0.00
Sheep veins at low (L) pressure					
LVCI	10	2312.49	56.40	−135.08	0.00
LVCS	12	1285.00	14.37	−16.75	0.00
LVF	30	2288.13	19.42	−76.38	0.00
LVJ	10	1931.50	15.73	5.68	0.00
Human vessels					
Fem	30	3482.06	30.97	−56.81	0.00
Saf	20	2087.20	49.14	−48.32	0.00

[a]Number of available sets of data for each type of vessel.

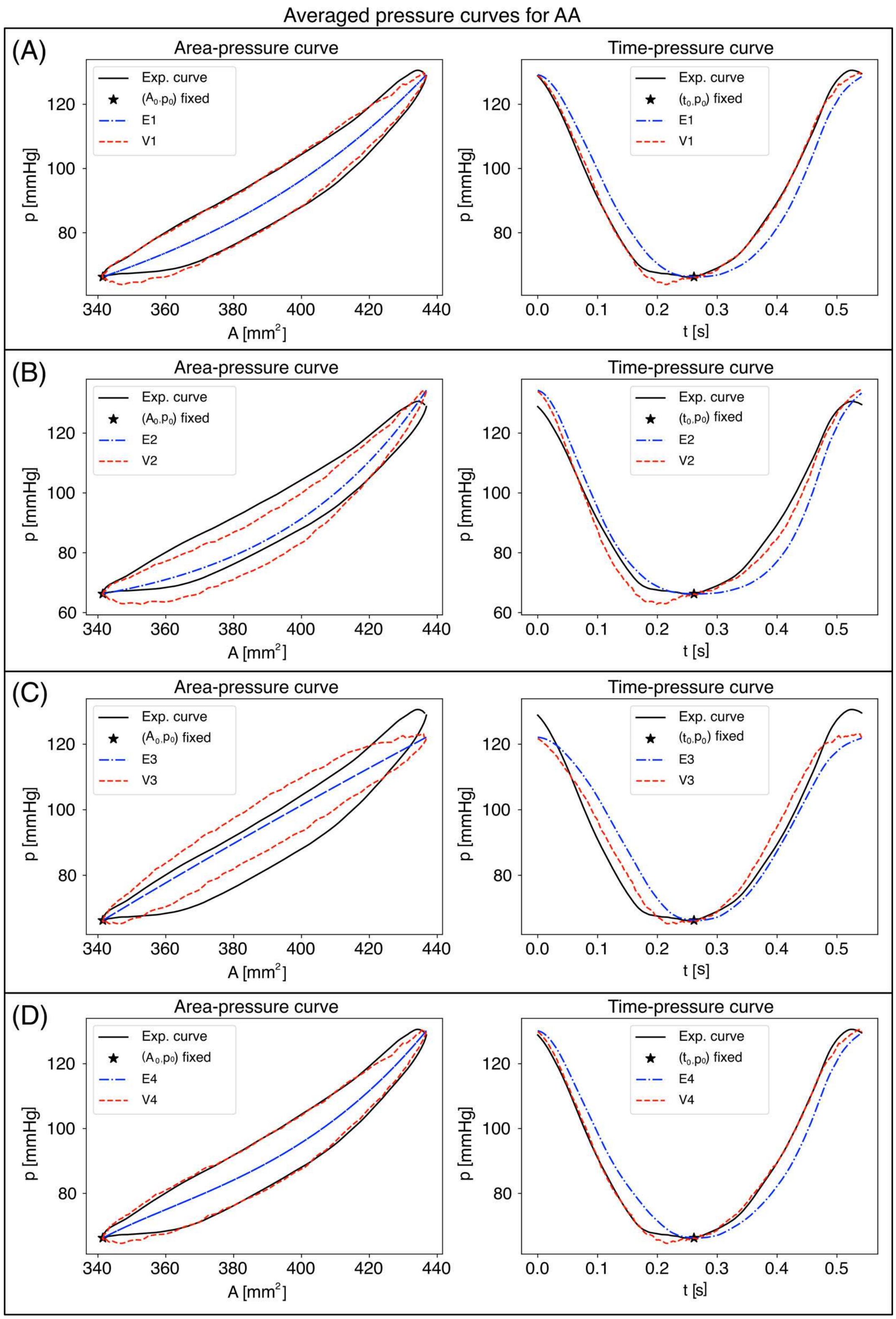

FIGURE A1 **Fitted pressure curves for AA.** Comparison between experimental and fitted pressure curves for all the estimation cases of an example dataset of AA. Black solid lines represent averaged experimental area-pressure and time–pressure curves, blue dash-dot lines represent the fitted curves obtained considering the elastic cases E1–E4, while red dashed lines represent the fitted curves obtain considering the viscoelastic cases V1–V4.

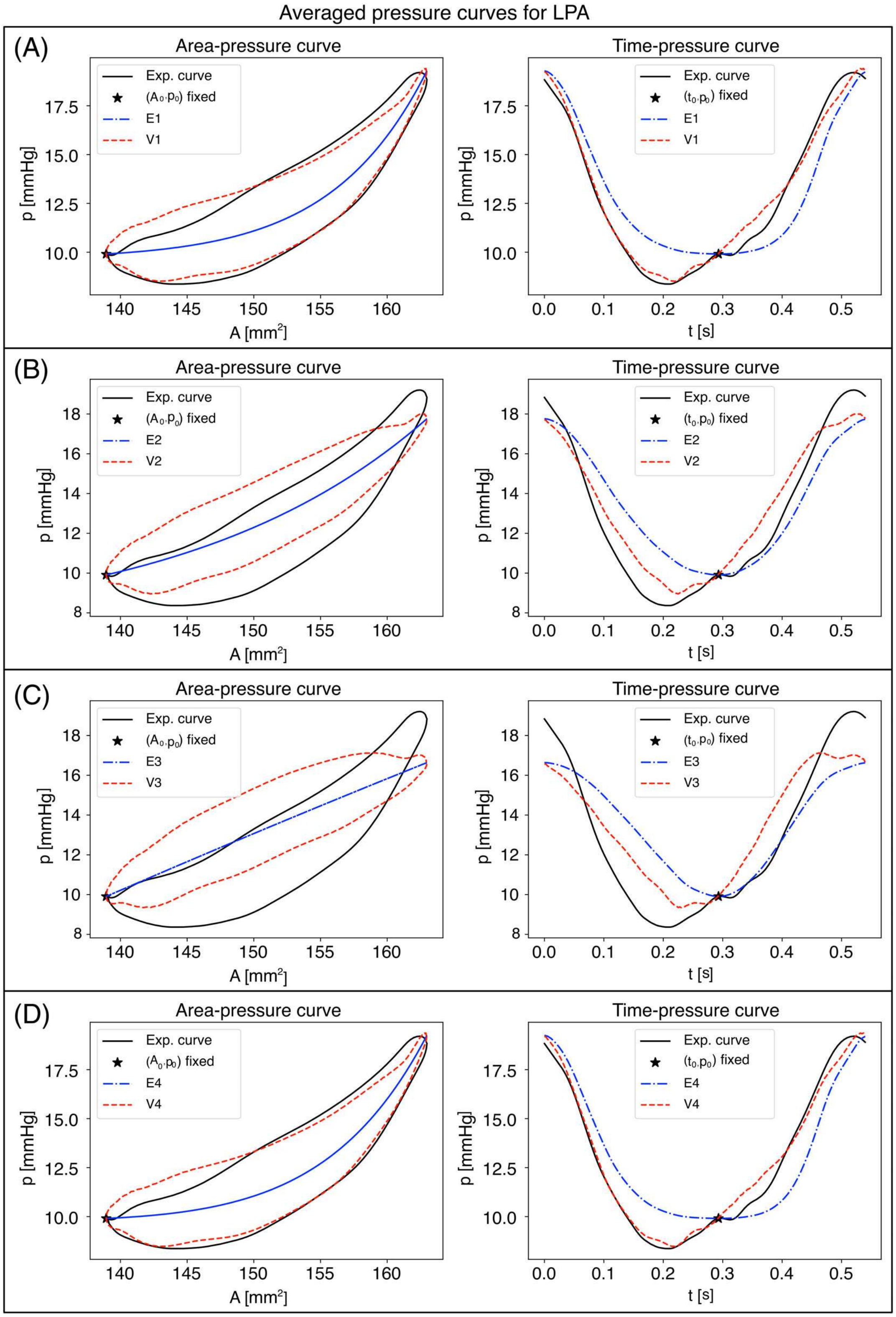

FIGURE A2 **Fitted pressure curves for LPA.** Comparison between experimental and fitted pressure curves for all the estimation cases of an example dataset of LPA. Black solid lines represent averaged experimental area-pressure and time–pressure curves, blue dash-dot lines represent the fitted curves obtained considering the elastic cases E1–E4, while red dashed lines represent the fitted curves obtain considering the viscoelastic cases V1–V4.

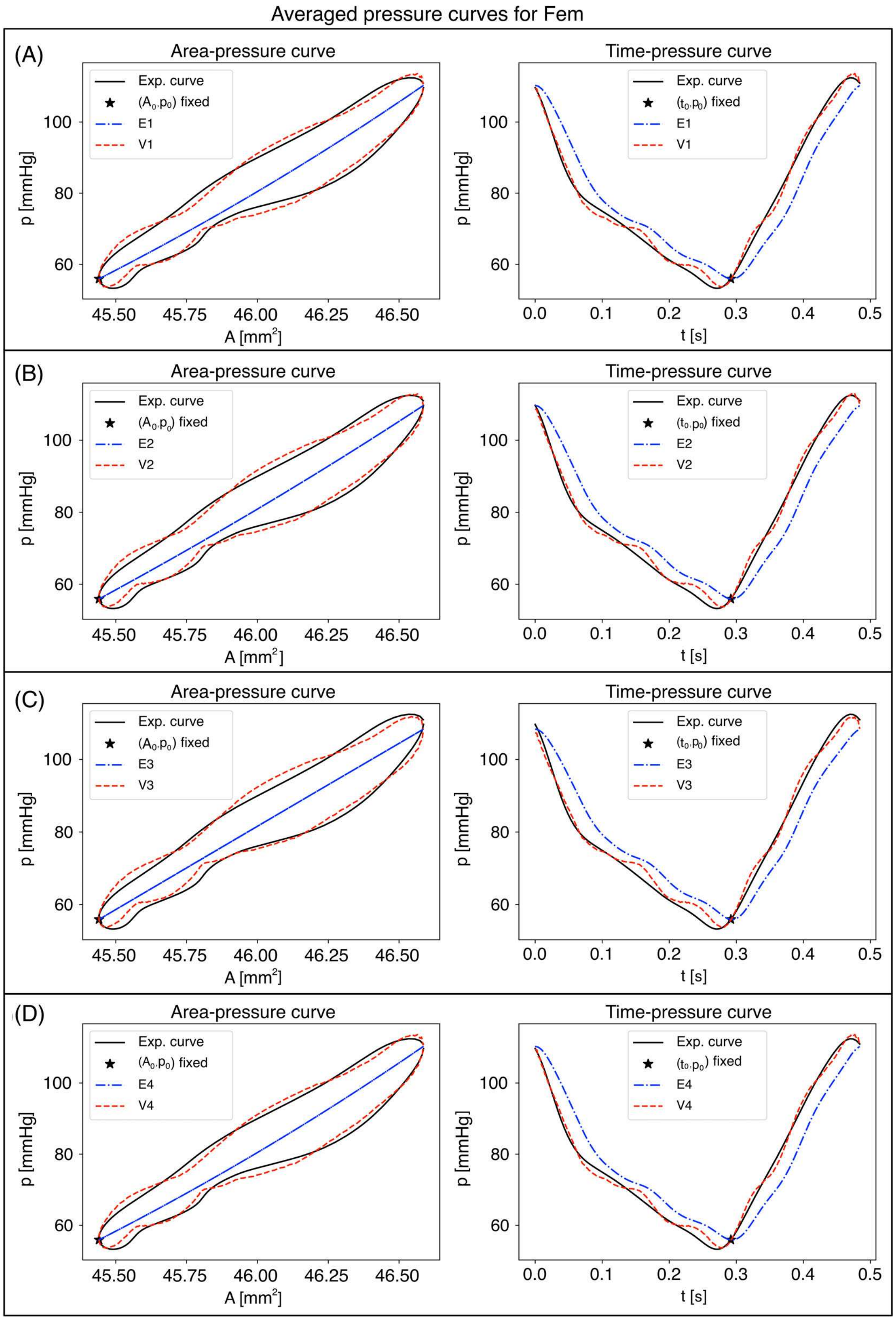

FIGURE A3 **Fitted pressure curves for Fem.** Comparison between experimental and fitted pressure curves for all the estimation cases of an example dataset of Fem. Black solid lines represent averaged experimental area-pressure and time–pressure curves, blue dash-dot lines represent the fitted curves obtained considering the elastic cases E1–E4, while red dashed lines represent the fitted curves obtain considering the viscoelastic cases V1–V4.